

# Magnetism in the single-band Hubbard model

T. Herrmann and W. Nolting

*Humboldt-Universität zu Berlin, Institut für Physik, Invalidenstr. 110, 10115 Berlin, Germany*  
(2.Sep.96; revised version 7.Jan.97)

A self-consistent spectral density approach (SDA) is applied to the Hubbard model to investigate the possibility of spontaneous ferro- and antiferromagnetism. Starting point is a two-pole ansatz for the single-electron spectral density, the free parameter of which can be interpreted as energies and spectral weights of respective quasiparticle excitations. They are determined by fitting exactly calculated spectral moments. The resulting self-energy consists of a local and a non-local part. The higher correlation functions entering the spin-dependent local part can be expressed as functionals of the single-electron spectral density. Under certain conditions for the decisive model parameters (Coulomb interaction  $U$ , Bloch-bandwidth  $W$ , band occupation  $n$ , temperature  $T$ ) the local part of the self-energy gives rise to a spin-dependent band shift, thus allowing for spontaneous band magnetism. As a function of temperature, second order phase transitions are found away from half filling, but close to half filling the system exhibits a tendency towards first order transitions. The non-local self-energy part is determined by use of proper two-particle spectral densities. Its main influence concerns a (possibly spin-dependent) narrowing of the quasiparticle bands with the tendency to stabilize magnetic solutions. The non-local self-energy part disappears in the limit of infinite dimensions. We present a full evaluation of the Hubbard model in terms of quasiparticle densities of states, quasiparticle dispersions, magnetic phase diagram, critical temperatures ( $T_C$ ,  $T_N$ ) as well as spin and particle correlation functions. Special attention is focused on the non-locality of the electronic self-energy, for which some rigorous limiting cases are worked out.

## I. INTRODUCTION

Important consequences of strong correlations in narrow energy bands as band magnetism, metal-insulator transitions or high- $T_C$  superconductivity are normally investigated by rather simplified theoretical models. Of special interest is the Hubbard model<sup>1</sup> which describes itinerant electrons in a single non-degenerate energy band interacting via an on-site Coulomb interaction  $U$ . It incorporates in the simplest way the interplay of the kinetic energy, the Coulomb interaction, the Pauli principle and the bandstructure and its consequences for the electronic and magnetic properties of the band system. Originally, the model was thought to explain the bandmagnetism of the transition metals and their compounds as well as the temperature, pressure or doping driven metal-insulator transition of some metal oxides. The latter were first recognized by Mott<sup>2</sup> as contradicting conventional band theory (Mott transition). It is to the merit of Hubbard<sup>3</sup>

to have demonstrated, how strong electron correlations may cause insulating behaviour of not fully occupied energy bands.

The in principle rather simple model provokes nevertheless a non-trivial many body problem, that could be solved up to now only for some special cases as, e.g., the ground state of the one-dimensional system<sup>4</sup>. Other rigorous statements concern the possibility of collective magnetic order in two and three-dimensional lattices<sup>5-7</sup>. In the first years after Hubbard's pioneering work, the investigation has mainly been focused on the existence of ferro- and antiferromagnetic solutions of the single-band model<sup>8,9</sup>, where, however, approximations had to be tolerated when tackling the respective magnetic phase diagram. The interest in the Hubbard model has got a dramatic upsurge in the recent past when its relevance to the high temperature superconductivity became manifest<sup>10</sup>. It has been recognized that in the limit of infinite dimensions  $d$  the electronic self-energy is wave-vector independent<sup>11-13</sup>. That simplifies but nevertheless does not solve the problem. Substantial progress has been made by the observation<sup>14-16</sup> that for  $d \rightarrow \infty$  the self-energy of the Hubbard model and the self-energy of the Anderson model are the same functionals of their respective local Green functions. However, up to now one does not know the exact functional form. With respect to the superconductivity problem, most of the recent investigations have been done for the half filled or almost half filled energy band. Compared to this, relatively little effort is concentrated on the search for magnetic solutions of the Hubbard model. Some interesting recent investigations which address the magnetic behaviour can be found in<sup>17-21</sup>.

Ferromagnetic solutions are to be expected, if at all, only in the strong coupling regime  $U/W > 1$  ( $W$ : Bloch-bandwidth). It has been demonstrated<sup>9,22</sup> that such strong electron correlations are reasonable well accounted for by the "spectral density approach" (SDA) which basically consists in a two-pole ansatz for the single-electron spectral density. The free parameters in the two-pole spectral density are self-consistently fixed by equating exactly calculated spectral moments. The advantages of the SDA rest on the clear and simple concept and its non-perturbative character. It turns out to be essentially equivalent to the Roth method<sup>8,23</sup> and to the Mori-projector formalism<sup>24,25</sup>. Various applications to Bose-, Fermi-, and classical systems<sup>26-28</sup> have proven the efficiency of the SDA. Previous applications of the SDA to the problem of band magnetism in the Hubbard model for the bulk<sup>22</sup> as well as for systems with reduced symmetry<sup>29</sup> have been restricted to a local self-energy that could be derived self-consistently. The wave-vector dependent part of the self-energy, being built

up by higher correlation functions referring to double hopping, spinflip and density correlations, has been neglected. Recently, the justification of such a neglect has been questioned<sup>23,30</sup> and investigated in detail for the paramagnetic two-dimensional system.

In this paper we present for the first time a full evaluation of the SDA to the Hubbard model with respect to the possibility of spontaneous ferro- and antiferromagnetism<sup>31</sup>. Special attention is devoted to the question to what extent the non-locality of the electronic self-energy influences the stability of magnetic order. For this purpose we have organized the paper as follows. In sec. II we give a short introduction to the underlying many body problem. The theory of the spectral density approach to the Hubbard model is developed in detail in Sec. III. In Sec. IV we derive some analytic expressions for the case of half-filling ( $n = 1$ ) and in the limit of strong Coulomb interaction  $U \rightarrow \infty$ . The results of the numerical calculations are discussed in Sec. V, where we investigate para-, ferro- as well as antiferromagnetic solutions. We discuss the properties of the system by means of a magnetic phase diagram, magnetization curves, critical temperatures, quasiparticle density of states and quasiparticle dispersions. In Sec. VI we give a short summary and some concluding remarks.

## II. MANY BODY PROBLEM

Starting point of our investigation is the single-band Hubbard model:

$$\mathcal{H} = \sum_{i,j,\sigma} (T_{ij} - \mu \delta_{ij}) c_{i\sigma}^\dagger c_{j\sigma} + \frac{U}{2} \sum_{i,\sigma} n_{i\sigma} n_{i-\sigma}. \quad (1)$$

$c_{i\sigma}^\dagger$  ( $c_{j\sigma}$ ) is the creation (annihilation) operator of an electron with spin  $\sigma = \uparrow, \downarrow$  in a Wannier state at lattice site  $\mathbf{R}_i$ .  $n_{i\sigma} = c_{i\sigma}^\dagger c_{i\sigma}$  is the number operator and  $U$  denotes the intraatomic Coulomb matrix element. The intersite hopping integrals  $T_{ij}$  are connected via Fourier transformation to the Bloch energies:

$$\varepsilon(\mathbf{k}) = \frac{1}{N} \sum_{i,j} T_{ij} e^{-i\mathbf{k}(\mathbf{R}_i - \mathbf{R}_j)}. \quad (2)$$

$N$  is the number of lattice sites. The center of gravity of the Bloch band is given by:

$$T_0 = \frac{1}{N} \sum_{\mathbf{k}} \varepsilon(\mathbf{k}) = T_{ii}. \quad (3)$$

Since the theory presented below does at this point not depend on the functional form of  $\varepsilon(\mathbf{k})$  we do not specify the underlying lattice. In sec. 5 we will discuss some numerical results for the bcc-lattice and the square lattice. Other lattice structures, such as sc, fcc, hc- $d=\infty$ , fcc- $d=\infty$  will be considered in a forthcoming paper<sup>32</sup>.

All interesting single-particle properties of the system are determined by the retarded single-electron Green function:

$$G_{\mathbf{k}\sigma}(E) = \langle\langle c_{\mathbf{k}\sigma}; c_{\mathbf{k}\sigma}^\dagger \rangle\rangle_E = \frac{1}{N} \sum_{i,j} e^{-i\mathbf{k}(\mathbf{R}_i - \mathbf{R}_j)} G_{ij\sigma}(E),$$

$$G_{ij\sigma}(E) = \langle\langle c_{i\sigma}; c_{j\sigma}^\dagger \rangle\rangle_E = -i \int_0^{+\infty} dt e^{-\frac{i}{\hbar} E t} \langle [c_{i\sigma}(t), c_{j\sigma}^\dagger(0)]_+ \rangle. \quad (4)$$

Here,  $\mathbf{k}$  is a wave-vector of the first Brillouin zone and  $c_{\mathbf{k}\sigma}$  the Fourier transform of  $c_{i\sigma}$ .  $[\dots]_{(+)-}$  denotes the (anti)commutator and  $\langle \dots \rangle$  the grand-canonical average.

By introducing the electronic self-energy  $\Sigma_{\mathbf{k}\sigma}(E)$  via the definition

$$\langle\langle \left[ c_{\mathbf{k}\sigma}, \frac{1}{2} U \sum_{i\sigma} n_{i\sigma} n_{i-\sigma} \right]_- ; c_{\mathbf{k}\sigma}^\dagger \rangle\rangle_E = \Sigma_{\mathbf{k}\sigma}(E) G_{\mathbf{k}\sigma}(E), \quad (5)$$

the equation of motion of the Green function is formally solved:

$$G_{\mathbf{k}\sigma}(E) = \frac{\hbar}{E - (\varepsilon(\mathbf{k}) - \mu) - \Sigma_{\mathbf{k}\sigma}(E)}. \quad (6)$$

The self-energy  $\Sigma_{\mathbf{k}\sigma}(E)$  therefore gathers all influences of the two particle interaction of the Hubbard model.

The approach to the Hubbard model in this paper is attached to the single-electron spectral density

$$S_{\mathbf{k}\sigma}(E) = -\frac{1}{\pi} \text{Im} G_{\mathbf{k}\sigma}(E), \quad (7)$$

which contains exactly the same information as the Green function or the self-energy. Via (inverse) photoemission the spectral density is directly related to the experiment.

By use of the spectral theorem one can determine from the spectral density the average occupation number:

$$\langle n_{i\sigma} \rangle = \langle c_{i\sigma}^\dagger c_{i\sigma} \rangle = \int_{-\infty}^{+\infty} dE f_-(E) S_{ii\sigma}(E - \mu) \quad (8)$$

$$= \int_{-\infty}^{+\infty} dE f_-(E) \rho_\sigma(E). \quad (9)$$

Here we have introduced the Fermi function  $f_-(E)$  and the quasi-particle density of states (QDOS):

$$\rho_\sigma(E) = \frac{1}{\hbar} S_{ii\sigma}(E - \mu) = \frac{1}{\hbar N} \sum_{\mathbf{k}} S_{\mathbf{k}\sigma}(E - \mu). \quad (10)$$

If we assume translational symmetry, the average occupation number does not depend on the lattice site  $\mathbf{R}_i$ :

$$n_\sigma = \langle n_{i\sigma} \rangle. \quad (11)$$

The total occupation number is given by  $n = n_\uparrow + n_\downarrow$ .

A lot of information about the spectral density can be drawn from its spectral decomposition (Lehmann representation)

$$S_{\mathbf{k}\sigma}(E) = \frac{\hbar}{\Xi} \sum_{n,m} |\langle E_n | c_{\mathbf{k}\sigma}^\dagger | E_m \rangle|^2 e^{-\beta E_n} (e^{\beta E} + 1) \times \delta[E - (E_n - E_m)], \quad (12)$$

where  $\Xi$  is the grand canonical partition function,  $|E_m\rangle$  an  $N$ -particle, and  $|E_n\rangle$  an  $(N+1)$ -particle eigenstate of the Hamiltonian. Therefore, the energy differences  $E_n - E_m$  correspond to the excitation energies required for adding a single electron to the  $N$ -particle system.

Central quantities of our procedure are the moments  $M_{\mathbf{k}\sigma}^{(n)}$  of the spectral density  $S_{\mathbf{k}\sigma}(E)$ , for which two equivalent representations exist. One is the usual definition via an energy integral

$$M_{\mathbf{k}\sigma}^{(n)} = \int_{-\infty}^{+\infty} dE E^n S_{\mathbf{k}\sigma}(E), \quad (13)$$

while the other involves only commutator relations between the construction operators and the Hamiltonian and is, therefore, independent of the spectral density itself:

$$M_{\mathbf{k}\sigma}^{(n)} = \frac{1}{N} \sum_{i,j} e^{-i\mathbf{k}\cdot(\mathbf{R}_i - \mathbf{R}_j)} \times \left\langle \underbrace{\left[ \dots [c_{i\sigma} \mathcal{H}]_- \dots, \mathcal{H} \right]}_{(n-p)\text{-times}} \underbrace{\left[ \mathcal{H}, \dots [\mathcal{H}, c_{j\sigma}^\dagger]_- \dots \right]}_{p\text{-times}} \right\rangle_+. \quad (14)$$

$p$  is an integer between 0 and  $n$  with  $n = 0, 1, 2, \dots$

Besides systems with translational symmetry we also want to investigate antiferromagnetic structures. For simplicity we restrict the analytical calculations presented in the next sections to the case of paramagnetism and ferromagnetism, respectively, and give only a brief idea of the extension to antiferromagnetism. The following is meant to introduce the notation necessary to describe antiferromagnetic configurations.

First we have to decompose the chemical lattice into two equivalent magnetic sublattices  $A$  and  $B$ . The original, chemical lattice can then be described by a so-called magnetic Bravais lattice ( $\mathbf{R}_i$ ) with a two-atomic basis ( $\mathbf{r}_\alpha$ ):

$$\mathbf{R}_{i\alpha} = \mathbf{R}_i + \mathbf{r}_\alpha, \quad (i = 1, \dots, N/2; \alpha = A, B) \quad (15)$$

This new labeling of the lattice sites applies, of course, for the creation and annihilation operators  $c_{i\alpha\sigma}^\dagger$ ,  $c_{i\alpha\sigma}$  as well.

If we assume translational symmetry inside the magnetic sublattices, expectation values do not depend on the lattice site  $\mathbf{R}_i$ . For example we write for the sublattice occupation number:

$$n_{\alpha\sigma} = \langle n_{i\alpha\sigma} \rangle = \langle c_{i\alpha\sigma}^\dagger c_{i\alpha\sigma} \rangle. \quad (16)$$

In the case of antiferromagnetic order, the dependence on the sublattice index  $\alpha$  becomes important and  $n_{A\sigma} = n_{B-\sigma}$  holds. This yields for the sublattice magnetization:

$$m_A = n_{A\uparrow} - n_{A\downarrow} = n_{B\downarrow} - n_{B\uparrow} = -m_B. \quad (17)$$

Paramagnetism and ferromagnetism can still be described by setting  $n_{A\sigma} = n_{B\sigma}$ .

All calculations are carried out in wave-vector space. The actual choice of the antiferromagnetic configuration, therefore, comes in through the single-electron energies  $\varepsilon_{\alpha\beta}(\mathbf{k})$  only:

$$\varepsilon_{\alpha\beta}(\mathbf{k}) = \frac{2}{N} \sum_{i,j} T_{ij}^{\alpha\beta} e^{-i\mathbf{k}\cdot(\mathbf{R}_i - \mathbf{R}_j)}. \quad (18)$$

### III. SPECTRAL DENSITY APPROACH

We use a self-consistent spectral density approach (SDA)<sup>9</sup> to find an approximate solution of the Hubbard Hamilton operator. The method is based on a physically motivated ansatz for the single-electron spectral density. The spectral density approach has proven to be very successful studying various many body problems such as Bose, Fermi and classical systems<sup>26-28</sup>. The main advantages of this method are the physically simple concept and the explicit non-perturbative character. Recent applications use the SDA successfully for the investigation of the attractive Hubbard model ( $U < 0$ )<sup>33</sup>, the t-J-model<sup>34</sup> and for studying systems with reduced dimension<sup>29</sup>, surface magnetism<sup>35</sup> and magnetism of thin films<sup>36</sup>. The SDA is believed to be a good starting point for the investigation of high temperature superconductivity<sup>23,37</sup>.

The work presented here, is mainly concerned with the magnetic properties of the Hubbard model. For the first time we give a complete evaluation of the SDA theory. The SDA can be divided into three major steps:

- (i) The crucial point is to find a physically reasonable ansatz for the spectral density. Some hints can be drawn, for example, from exactly known limiting cases, sum rules for the peaks of the spectral density, spectral decompositions, etc.
- (ii) the mathematical ansatz in (i) will contain some free parameters, which can be fitted by the exactly calculated moments  $M_{\mathbf{k}\sigma}^{(n)}$  of the spectral density. All correlation functions, however, which occur in this procedure, have to be re-expressed by the spectral density.
- (iii) With (i) and (ii) one obtains a closed set of equations, which can be solved self-consistently.

If at all, ferromagnetism in the Hubbard model is to be expected in the strong correlation limit  $U > W$ . Therefore, our ansatz for the spectral density should be motivated in this limit. In the strict  $W = 0$  case, where no hopping is allowed between the lattice sites, the spectral density consists of two weighted  $\delta$ -functions. The two  $\delta$ -peaks are located at the energies  $T_0 - \mu$  and  $T_0 + U - \mu$ , corresponding to the excitation energies required to add

a ( $\sigma$ )-electron to a lattice site where a ( $-\sigma$ )-electron is already present or not.

The interesting question is what happens, if one allows for a small but non-zero hopping? Following Harris and Lange<sup>38</sup>, four effects are to be expected: A broadening of the  $\delta$ -peaks, a shift of the center of gravity of the peaks, a rearrangement of spectral weight between the peaks and, finally, the appearance of new, so-called "satellite" peaks near the energies  $E_{p,U} = T_0 + p \cdot U - \mu$  (with  $p \in \mathbb{Z} \setminus \{0,1\}$ ). The first three effects can already be seen in a two site Hubbard model. Harris and Lange have shown<sup>38</sup>, that the two satellite peaks at  $E_{-U}$  and  $E_{2,U}$ , which are closest to the main peaks, have weight factors of order  $(W/U)^4$ , being therefore negligible for the strongly correlated system ( $U \gg W$ ). The weights of the other satellite peaks are even smaller. Therefore, we can conclude that, in the case of strong correlation the spectral density has a two peak structure. Besides the Kondo-like peak, which is beyond the scope of our present investigation<sup>39</sup>, this decisive point in our theory is confirmed, for example, by recent calculations in the limit of infinite lattice dimensions  $d = \infty$ <sup>15,40</sup>.

If we neglect quasiparticle damping effects, the following two-pole ansatz for the single-electron spectral density is, therefore, physically reasonable:

$$S_{\mathbf{k}\sigma}(E) = \hbar \sum_{j=1,2} \alpha_{j\sigma}(\mathbf{k}) \delta(E - E_{j\sigma}(\mathbf{k}) + \mu). \quad (19)$$

The four free parameters  $E_{1\sigma}(\mathbf{k})$ ,  $E_{2\sigma}(\mathbf{k})$ ,  $\alpha_{1\sigma}(\mathbf{k})$ ,  $\alpha_{2\sigma}(\mathbf{k})$  contained in the ansatz (19) can be calculated using the two independent representations (13) and (14) of the spectral moments. For this we have to calculate the first four moments  $M_{\mathbf{k}\sigma}^{(0)} - M_{\mathbf{k}\sigma}^{(3)}$ , which are given, for example, in ref.<sup>9</sup>. After a straightforward calculation we finally get:

$$E_{(1,2)\sigma}(\mathbf{k}) = \frac{1}{2} \left[ B_{\mathbf{k}-\sigma} + U + \varepsilon(\mathbf{k}) \mp \sqrt{(B_{\mathbf{k}-\sigma} + U - \varepsilon(\mathbf{k}))^2 + 4Un_{-\sigma}(\varepsilon(\mathbf{k}) - B_{\mathbf{k}-\sigma})} \right], \quad (20)$$

$$\alpha_{1\sigma}(\mathbf{k}) = \frac{E_{2\sigma}(\mathbf{k}) - \varepsilon(\mathbf{k}) - Un_{-\sigma}}{E_{2\sigma} - E_{1\sigma}}, \quad (21)$$

$$\alpha_{2\sigma}(\mathbf{k}) = \frac{Un_{-\sigma} + \varepsilon(\mathbf{k}) - E_{1\sigma}(\mathbf{k})}{E_{2\sigma} - E_{1\sigma}} = 1 - \alpha_{1\sigma}(\mathbf{k}). \quad (22)$$

Here, we introduced the correction term  $B_{\mathbf{k}-\sigma}$ , which contains higher correlation functions (see below). The correction term  $B_{\mathbf{k}-\sigma}$  turns out to be of decisive importance with respect to the possibility of spontaneous magnetic order. We want to emphasize, that (20)-(22) reproduce the exact results obtained by Harris and Lange<sup>38</sup> in the strong correlation limit.

It is also interesting to look at the self-energy  $\Sigma_{\mathbf{k}\sigma}^{SDA}(E)$ , which is connected to the spectral density via:

$$S_{\mathbf{k}\sigma}(E) = \hbar \delta(E - \Sigma_{\mathbf{k}\sigma}(E) + \mu). \quad (23)$$

Using (20)-(22) we find:

$$\Sigma_{\mathbf{k}\sigma}^{SDA}(E) = Un_{-\sigma} \frac{E + \mu - B_{\mathbf{k}-\sigma}}{E + \mu - B_{\mathbf{k}-\sigma} - U(1 - n_{-\sigma})}. \quad (24)$$

Replacing  $B_{\mathbf{k}-\sigma}$  in (24) simply by the center of gravity  $T_0$  of the Bloch band, reduces  $\Sigma_{\mathbf{k}\sigma}^{SDA}(E)$  to the so-called Hubbard-I self-energy<sup>1</sup>. It is well known that the Hubbard-I solution is not able to describe ferromagnetism. The main shortcoming of the Hubbard-I solution with respect to the possibility of spontaneous magnetic order is the fact, that the centers of gravity of the quasiparticle subbands (so-called Hubbard bands) in the QDOS are spin-independent. Allowing for such a spin-dependence via the correction term  $B_{\mathbf{k}-\sigma}$  is the decisive improvement of the SDA upon the Hubbard-I solution.

The correction term  $B_{\mathbf{k}-\sigma}$  can be split into a  $\mathbf{k}$ -independent and a  $\mathbf{k}$ -dependent term:

$$B_{\mathbf{k}-\sigma} = B_{-\sigma} + F_{\mathbf{k}-\sigma}. \quad (25)$$

Assuming translational invariance and hopping between nearest neighbours only, the  $\mathbf{k}$ -dependence can be separated:

$$F_{\mathbf{k}-\sigma} = (\varepsilon(\mathbf{k}) - T_0)F_{-\sigma}. \quad (26)$$

The remaining terms  $B_{-\sigma}$  and  $F_{-\sigma}$  are given by:

$$B_{-\sigma} - T_0 = \frac{1}{n_{-\sigma}(1 - n_{-\sigma})} \frac{1}{N} \sum_{i,j}^{i \neq j} T_{ij} \langle c_{i-\sigma}^\dagger c_{j-\sigma} (2n_{i\sigma} - 1) \rangle, \quad (27)$$

$$F_{-\sigma} = \frac{1}{n_{-\sigma}(1 - n_{-\sigma})} [F_{-\sigma}^{(1)} + F_{-\sigma}^{(2)} + F_{-\sigma}^{(3)}] \quad (28)$$

$$F_{-\sigma}^{(1)} = \langle n_{i-\sigma} n_{j-\sigma} \rangle - n_{-\sigma}^2 \quad \text{"density correlation"}, \quad (29)$$

$$F_{-\sigma}^{(2)} = -\langle c_{j\sigma}^\dagger c_{j-\sigma}^\dagger c_{i-\sigma} c_{i\sigma} \rangle \quad \text{"double hopping cor."}, \quad (30)$$

$$F_{-\sigma}^{(3)} = -\langle c_{j\sigma}^\dagger c_{i-\sigma}^\dagger c_{j-\sigma} c_{i\sigma} \rangle \quad \text{"spinflip correlation"}. \quad (31)$$

The so-called spin dependent bandshift  $B_{-\sigma}$  may lead to an energy shift in the spin-spectra, allowing, therefore, for an exchange splitting between the spin-up and spin-down spectrum.

In former investigations of the magnetic properties of the Hubbard model within the SDA, the bandwidth correction  $F_{\mathbf{k}-\sigma}$  was neglected and only the local part of the self-energy was taken into account (see for example refs.<sup>22,29,33,35,36,41,42</sup>). The bandwidth correction was identified to be of minor importance with respect to spontaneous magnetism, because the last two correlation functions  $F_{-\sigma}^{(2)}$  and  $F_{-\sigma}^{(3)}$  are effectively spin independent. Further, the sum of  $F_{\mathbf{k}-\sigma}$  over all wave-vectors of the first Brillouin zone vanishes, so no additional exchange splitting is to be expected. In the widely discussed case of infinite dimensions ( $d = \infty$ ) the self-energy becomes local, i.e.,  $F_{\mathbf{k}-\sigma}$  vanishes. Many approximations for the three-dimensional Hubbard model also use a local self-energy for simplicity. Nevertheless, in three and lower dimensions the spin and wave-vector dependent bandwidth

correction  $F_{\mathbf{k}-\sigma}$  can induce substantial changes in the shape and the width of the QDOS. Since magnetism is favoured by narrow energy bands, the bandwidth correction may also have a significant influence on the magnetic behaviour. One major part of this work is concerned with the influence of the non-locality ( $\mathbf{k}$ -dependence) of the self-energy in three and lower dimensions. In particular, the influence of these non-local terms on the magnetic behaviour will be discussed.

In one and two dimensions Beenen and Edwards<sup>23</sup> and Mehlig et. al.<sup>37</sup> showed for the case of paramagnetism, that the inclusion of the  $\mathbf{k}$ -dependence leads to a rather good agreement of the quasiparticle dispersion calculated with the SDA and recent quantum Monte Carlo and exact diagonalization results<sup>43,44</sup>.

One of the more crude approximations in the ansatz (19) for the spectral density is the fact, that quasiparticle damping is not included. The imaginary part of the self-energy (24), therefore, is identical to zero. Since the magnetic variables, like the magnetization  $m$ , are given by an energy integration over the spectral density, the broadening of the peaks in the spectral density should not be very important. However, one has to take this question seriously. In a recent paper<sup>45</sup>, we investigated the influence of quasiparticle damping on the magnetic stability by a proper combination of the SDA and the coherent potential approximation. Guided by exact results in the strong coupling limit, we proposed a modified alloy analogy, which allows for spontaneous ferromagnetic solutions. Although in the paramagnetic case the results obtained by the modified alloy analogy are almost identical to the SDA-predictions, the region where the system exhibits ferromagnetism is strongly reduced if quasiparticle damping is included<sup>45</sup>. Further work on the influence of damping with respect to magnetism is in progress.

What remains to be done in order to get a closed set of equations is to express the two terms  $B_{-\sigma}$  and  $F_{-\sigma}$  by means of the spectral density:

**Spin-dependent bandshift:** The higher correlation function  $\langle n_{i\sigma} c_{i-\sigma}^\dagger c_{j-\sigma} \rangle$  which appears in the spin-dependent bandshift  $B_{-\sigma}$  is exactly determined by the single-electron spectral density<sup>41,22</sup>:

$$\langle n_{i\sigma} c_{i-\sigma}^\dagger c_{j-\sigma} \rangle = \frac{1}{UN\hbar} \sum_{\mathbf{k}} e^{-i\mathbf{k} \cdot (\mathbf{R}_i - \mathbf{R}_j)} \times \int_{-\infty}^{+\infty} dE f_{-}(E) [E - \varepsilon(\mathbf{k})] S_{\mathbf{k}-\sigma}(E - \mu). \quad (32)$$

This leads, together with the hopping correlation function  $\langle c_{i-\sigma}^\dagger c_{j-\sigma} \rangle$ , which is given directly by the spectral theorem

$$\langle c_{i-\sigma}^\dagger c_{j-\sigma} \rangle = \frac{1}{N\hbar} \sum_{\mathbf{k}} e^{-i\mathbf{k} \cdot (\mathbf{R}_i - \mathbf{R}_j)} \int_{-\infty}^{+\infty} dE f_{-}(E) S_{\mathbf{k}-\sigma}(E - \mu), \quad (33)$$

to the final expression for  $B_{-\sigma}$ :

$$B_{-\sigma} - T_0 = \frac{1}{n_{-\sigma}(1 - n_{-\sigma})} \frac{1}{N} \sum_{\mathbf{k}} \int_{-\infty}^{+\infty} dE f_{-}(E) (\varepsilon(\mathbf{k}) - T_0) \times \left[ \frac{2}{U} [E - \varepsilon(\mathbf{k})] - 1 \right] S_{\mathbf{k}-\sigma}(E - \mu). \quad (34)$$

**Bandwidth correction:** The evaluation of the higher correlation functions contained in the bandwidth correction  $F_{-\sigma}$  turns out to be more difficult. For simplicity we restrict the detailed calculation to the case of the spinflip correlation function  $F_{-\sigma}^{(3)}$ . The evaluation of the density and the double hopping correlation functions follows exactly the same line.

First we rewrite  $F_{-\sigma}^{(3)}$  as:

$$F_{-\sigma}^{(3)} = - \sum_l \delta_{lj} \langle c_{l\sigma}^\dagger c_{j+\Delta-\sigma}^\dagger c_{j-\sigma} c_{j+\Delta\sigma} \rangle, \quad (35)$$

where  $\Delta = \mathbf{R}_i - \mathbf{R}_j$  is a lattice vector which connects two neighbouring lattice sites. In the following we assume translational invariance and hopping only between nearest neighbours. Therefore,  $F_{-\sigma}^{(3)}$  does not depend on the explicit value of  $\Delta$ .

If we now introduce the higher spectral density  $A_{\mathbf{k}\sigma}^{(3)}$  via

$$A_{\mathbf{k}\sigma}^{(3)} = \frac{1}{N} \sum_{i,j} \int_{-\infty}^{+\infty} d(t-t') e^{-i\mathbf{k} \cdot (\mathbf{R}_i - \mathbf{R}_j)} e^{\frac{i}{\hbar} E(t-t')} A_{jl\sigma}^{(3)}(t-t'), \quad (36)$$

$$A_{jl\sigma}^{(3)}(t-t') = \frac{1}{2\pi} \langle [c_{j+\Delta-\sigma}^\dagger c_{j-\sigma} c_{j+\Delta\sigma}(t), c_{l\sigma}^\dagger(t')] \rangle_+, \quad (37)$$

it follows from the spectral theorem that  $F_{-\sigma}^{(3)}$  is given by:

$$F_{-\sigma}^{(3)} = - \frac{1}{N} \sum_{\mathbf{k}} \int_{-\infty}^{+\infty} dE f_{-}(E) A_{\mathbf{k}\sigma}^{(3)}(E - \mu). \quad (38)$$

To get further information about the structure of  $A_{\mathbf{k}\sigma}^{(3)}$ , we look at its spectral decomposition:

$$A_{\mathbf{k}\sigma}^{(3)}(E) = \frac{\hbar}{\Xi} \sum_{n,m} \langle E_n | \frac{1}{\sqrt{N}} \sum_j e^{i\mathbf{k} \cdot \mathbf{R}_j} c_{j+\Delta-\sigma}^\dagger c_{j-\sigma} c_{j+\Delta\sigma} | E_m \rangle \times \langle E_m | c_{\mathbf{k}\sigma}^\dagger | E_n \rangle e^{-\beta E_n} (e^{\beta E} + 1) \delta[E - (E_n - E_m)]. \quad (39)$$

The matrix elements  $\langle E_n | \dots | E_m \rangle$  determine the weight of  $A_{\mathbf{k}\sigma}^{(3)}(E)$  at the excitation energies  $E = E_n - E_m$ . Therefore  $A_{\mathbf{k}\sigma}^{(3)}(E)$  is non-zero only if the corresponding matrix elements do not vanish. Since (39) and the spectral decomposition of  $S_{\mathbf{k}\sigma}(E)$  (12) involve the same matrix element  $\langle E_m | c_{\mathbf{k}\sigma}^\dagger | E_n \rangle$ , the excitation energies  $E_n - E_m$  are exactly the same as in  $S_{\mathbf{k}\sigma}(E)$ . It is, therefore, reasonable to assume that the positions of the quasiparticle peaks in  $A_{\mathbf{k}\sigma}^{(3)}(E)$  are also the same as in

$S_{\mathbf{k}\sigma}(E)$ . However, because the other matrix element in (39) is not equal to the one in (12), the distribution of spectral weight over the peaks will be different in  $A_{\mathbf{k}\sigma}^{(3)}(E)$  and  $S_{\mathbf{k}\sigma}(E)$ . We can, therefore, formulate an ansatz for  $A_{\mathbf{k}\sigma}^{(3)}(E)$ :

$$A_{\mathbf{k}\sigma}^{(3)}(E) = \hbar \sum_{j=1,2} \beta_{j\sigma}^{(3)}(\mathbf{k}) \delta(E - E_{j\sigma}(\mathbf{k}) + \mu), \quad (40)$$

where  $E_{j\sigma}(\mathbf{k})$  ( $j = 1, 2$ ) are the "old" positions of the peaks given by (20) and  $\beta_{j\sigma}^{(3)}(\mathbf{k})$  the "new" weight factors which have to be determined. As in the case of  $S_{\mathbf{k}\sigma}(E)$  this can easily be done by evaluating the first two spectral moments of  $A_{\mathbf{k}\sigma}^{(3)}(E)$ . Note, that the same procedure yields the exact result (32) when applied to the higher correlation function  $\langle n_{i\sigma} c_{i-\sigma}^\dagger c_{j-\sigma} \rangle$  involved in the bandshift  $B_{-\sigma}$ .

After a lengthy but straightforward calculation we find via (38) the final expression for the three higher correlation functions  $F_{-\sigma}^{(1,2,3)}$ :

$$F_{-\sigma}^{(1)} = -\frac{\eta_{-\sigma} \langle c_{i-\sigma}^\dagger c_{j-\sigma} \rangle + \nu_{-\sigma} \langle n_{i\sigma} c_{i-\sigma}^\dagger c_{j-\sigma} \rangle}{1 + \nu_{0\sigma} \nu_{0-\sigma}}, \quad (41)$$

$$F_{-\sigma}^{(2)} = -\frac{(\eta_{-\sigma} + \nu_{-\sigma}) \langle c_{i-\sigma}^\dagger c_{j-\sigma} \rangle - \nu_{-\sigma} \langle n_{i\sigma} c_{i-\sigma}^\dagger c_{j-\sigma} \rangle}{1 - \nu_{0\sigma}}, \quad (42)$$

$$F_{-\sigma}^{(3)} = -\frac{\eta_{-\sigma} \langle c_{i-\sigma}^\dagger c_{j-\sigma} \rangle + \nu_{-\sigma} \langle n_{i\sigma} c_{i-\sigma}^\dagger c_{j-\sigma} \rangle}{1 + \nu_{0\sigma}}. \quad (43)$$

For simplicity we introduced the abbreviations:

$$\eta_{-\sigma} = \frac{1}{1 - n_{-\sigma}} \left[ \langle c_{i-\sigma}^\dagger c_{j-\sigma} \rangle - \langle n_{i-\sigma} c_{i\sigma}^\dagger c_{j\sigma} \rangle \right], \quad (44)$$

$$\nu_{-\sigma} = \frac{1}{n_{-\sigma}(1 - n_{-\sigma})} \left[ \langle n_{i-\sigma} c_{i\sigma}^\dagger c_{j\sigma} \rangle - n_{-\sigma} \langle c_{i\sigma}^\dagger c_{j\sigma} \rangle \right], \quad (45)$$

$$\nu_{0\sigma} = \frac{\langle n_{i\sigma} n_{i-\sigma} \rangle - n_{\sigma} n_{-\sigma}}{n_{-\sigma}(1 - n_{-\sigma})}. \quad (46)$$

Since  $\langle n_{i-\sigma} c_{i\sigma}^\dagger c_{j\sigma} \rangle$  and  $\langle c_{i-\sigma}^\dagger c_{j-\sigma} \rangle$  are given by (32) and (33), respectively, the bandwidth correction  $F_{-\sigma}$  can be calculated by means of the single-electron spectral density  $S_{\mathbf{k}\sigma}(E)$  only. Equations (19)-(22), (25), (32)-(34) and (41)-(46) build a closed set of equations which can be solved self-consistently.

Expressions (41)-(46) for the bandwidth correction are identical to the ones obtained by the method introduced by Roth<sup>8</sup>, both methods being, therefore, equivalent.

For the extension of the theory to antiferromagnetic systems, we use an effective medium approach described in ref.<sup>42</sup>. Since all further calculations are strictly along the lines of<sup>42</sup> we do not give any details here.

**Paramagnetic static susceptibility:** A lot of information about the magnetic behaviour of the system can be drawn from the static susceptibility:

$$\chi(n, T, H) = \frac{1}{\mu_0} \left( \frac{\partial M}{\partial H} \right)_T. \quad (47)$$

$\mu_0$  is the vacuum permeability,  $H$  denotes a static magnetic field and

$$M = \frac{N}{V} \mu_B (n_\uparrow - n_\downarrow) \quad (48)$$

is the magnetization of the system.

For studying magnetic phase transitions we are interested in the static susceptibility in the limit  $H \rightarrow 0$ :

$$\chi^{(0)}(n, T) = \frac{1}{\mu_0} \left( \frac{\partial M}{\partial H} \right)_T \Big|_{\text{paramag., } H=0}. \quad (49)$$

The poles of the paramagnetic static susceptibility  $\chi^{(0)}(n, T)$  indicate the instabilities of the system against ferromagnetic order. Therefore, all second order phase transitions from paramagnetism to ferromagnetism can be read off from  $\chi^{(0)}(n, T)$ , which needs as an input only the paramagnetic solution. Besides this, the paramagnetic Curie temperature  $\Theta$  as well as the critical exponent  $\gamma$  of the susceptibility can easily be obtained from  $\chi^{(0)}(n, T)$ <sup>46</sup>.

To calculate the static susceptibility we have to include a Zeeman term

$$H_Z = -\mu_B H (n_{i\uparrow} - n_{i\downarrow}) \quad (50)$$

in the Hamiltonian (1), which couples the magnetic field  $H$  to the local magnetic moment  $m_i = n_{i\uparrow} - n_{i\downarrow}$ . This additional term does not alter or complicate the theory presented above. However, when differentiating the magnetization with respect to the magnetic field, we have to take into account that all expectation values are implicit functions of  $H$ <sup>46</sup>. All calculations can be done analytically, whereas the results are rather lengthy.

#### IV. LIMITING CASES

Before we discuss the results of the numerical evaluation of the theory, we want to develop some analytical results for the case of exact half filling  $n = 1$  and for the limit of strong Coulomb interaction  $U \rightarrow \infty$ . Both terms, the bandshift  $B_{-\sigma}$  and the bandwidth correction  $F_{-\sigma}$  simplify considerably in these cases. Throughout this section we assume translational invariance, hopping between nearest neighbours only and a symmetric BDOS.

First we consider the two correlation functions  $\langle n_{i-\sigma} c_{i\sigma}^\dagger c_{j\sigma} \rangle$  and  $\langle c_{i-\sigma}^\dagger c_{j-\sigma} \rangle$  which are given by (32) and (33) respectively. The process described by  $\langle n_{i-\sigma} c_{i\sigma}^\dagger c_{j\sigma} \rangle$  can be understood as a hopping process of a  $(\sigma)$ -electron with the condition that one of the sites is occupied by a  $(-\sigma)$ -electron. Because of the required double occupancy this process is suppressed in the limit of large  $U$  and  $n \leq 1$ . With (32) and (19)-(22) we find indeed:

$$\langle c_{i-\sigma}^\dagger c_{j-\sigma} n_{i\sigma} \rangle \xrightarrow{n \leq 1, U \rightarrow \infty} 0. \quad (51)$$

For the half-filled band, paramagnetism and  $T = 0\text{K}$ , a simple analytical calculation involving (32), (33) and (19)-(22) yields the relation:

$$\langle c_{i-\sigma}^\dagger c_{j-\sigma} n_{i\sigma} \rangle = \frac{1}{2} \langle c_{i-\sigma}^\dagger c_{j-\sigma} \rangle. \quad (52)$$

As  $U \rightarrow \infty$  for the case of half filling the hopping correlation  $\langle c_{i-\sigma}^\dagger c_{j-\sigma} \rangle$  should vanish, because all hopping processes require an energetically unfavoured double occupancy. In fact, (20)-(22) in (33) give for ( $i \neq j$ ):

$$\langle c_{i-\sigma}^\dagger c_{j-\sigma} \rangle \xrightarrow{n=1, U \rightarrow \infty} 0. \quad (53)$$

We now want to focus on the spin-dependent bandshift  $B_{-\sigma}$  and the bandwidth correction  $F_{-\sigma}$  in four different limiting cases:

**(i) Large  $U$  and less than half filling:** With (51) the bandshift  $B_{-\sigma}$  is given by:

$$B_{-\sigma} \xrightarrow{n < 1, U \rightarrow \infty} -\frac{Z_1 T_1}{n_{-\sigma}(1 - n_{-\sigma})} \langle c_{i-\sigma}^\dagger c_{j-\sigma} \rangle + T_0. \quad (54)$$

$Z_1$  is the number of nearest neighbours and  $T_1$  denotes the hopping integral between neighbouring lattice sites. It is interesting to notice that in the large  $U$  limit the bandshift of the ( $\sigma$ )-band being proportional to  $B_{-\sigma}$  is mainly determined by the hopping of the ( $-\sigma$ )-quasiparticles.

The density, double-hopping and spinflip correlation functions reduce in this limit to:

$$F_{-\sigma}^{(1)} \xrightarrow{n < 1, U \rightarrow \infty} -(1 - n_{-\sigma}) \frac{\langle c_{i-\sigma}^\dagger c_{j-\sigma} \rangle^2}{1 - n}, \quad (55)$$

$$F_{-\sigma}^{(2)} \xrightarrow{n < 1, U \rightarrow \infty} 0, \quad (56)$$

$$F_{-\sigma}^{(3)} \xrightarrow{n < 1, U \rightarrow \infty} -\frac{\langle c_{i\sigma}^\dagger c_{j\sigma} \rangle \langle c_{i-\sigma}^\dagger c_{j-\sigma} \rangle}{1 - n}. \quad (57)$$

**(ii) Paramagnetism, large  $U$  and less than half filling:** In the case of paramagnetism we can combine (55)-(57), which yields for the bandwidth correction  $F_{-\sigma}$ :

$$F_{-\sigma} \xrightarrow{n < 1, U \rightarrow \infty} \frac{4}{n(2 - n)} \left[ -\left(2 - \frac{n}{2}\right) \frac{\langle c_{i\sigma}^\dagger c_{j\sigma} \rangle^2}{1 - n} \right]. \quad (58)$$

By introducing the spin-spin correlation function  $\langle \mathbf{S}_i \mathbf{S}_j \rangle$  this can be written as:

$$F_{-\sigma} \xrightarrow{n < 1, U \rightarrow \infty} \frac{4}{n(2 - n)} \left[ \langle \mathbf{S}_i \mathbf{S}_j \rangle - \frac{\langle c_{i\sigma}^\dagger c_{j\sigma} \rangle^2}{2} \right]. \quad (59)$$

Here, the spin-spin correlation function is defined in the usual way:

$$\langle \mathbf{S}_i \mathbf{S}_j \rangle = \frac{1}{2} \langle S_i^+ S_j^- \rangle + \frac{1}{2} \langle S_i^- S_j^+ \rangle + \langle S_i^z S_j^z \rangle, \quad (60)$$

with:

$$S_i^+ = c_{i\uparrow}^\dagger c_{i\downarrow}, \quad S_i^- = c_{i\downarrow}^\dagger c_{i\uparrow}, \quad S_i^z = \frac{1}{2} (n_{i\uparrow} - n_{i\downarrow}). \quad (61)$$

**(iii) Paramagnetism and half filling:** For the exact half filled band ( $n = 1$ ) we can use (52) to simplify the expressions for  $B_{-\sigma}$  and  $F_{-\sigma}$ :

$$B_{-\sigma} = T_0 \quad (62)$$

$$F_{-\sigma} = \frac{12}{n(2 - n)} \left[ -\frac{\langle c_{i\sigma}^\dagger c_{j\sigma} \rangle^2}{8 \langle n_{i\sigma} n_{i-\sigma} \rangle - 16 \langle n_{i\sigma} n_{i-\sigma} \rangle^2} \right]. \quad (63)$$

**(iv) Paramagnetism, half filling and large  $U$ :** If we perform the large  $U$  limit starting from the exact expression (63) for  $F_{-\sigma}$ , a straightforward calculation yields:

$$F_{-\sigma} \xrightarrow{n=1, U \rightarrow \infty} -\frac{3}{Z_1}. \quad (64)$$

At this point we want to emphasize that  $n \rightarrow 1$  and the limit  $U \rightarrow \infty$  do not commute. This can easily be seen with the following relation for the hopping correlation function which is valid for  $n \leq 1$  and  $U \rightarrow \infty$ :

$$\langle c_{i\sigma}^\dagger c_{j\sigma} \rangle \leq \frac{-1}{Z_1 T_1} (1 - n). \quad (65)$$

Therefore, expression (58) for  $F_{-\sigma}$  vanishes as  $n \rightarrow 1$  contrary to the correct result given by (64).

## V. DISCUSSION AND RESULTS

The calculations in three dimensions are done for a lattice with bcc structure with the tight-binding dispersion given by:

$$\varepsilon(\mathbf{k}) = Z_1 T_1 \cos(k_x a) \cos(k_y a) \cos(k_z a) + T_0. \quad (66)$$

$a$  is the lattice constant,  $Z_1$  the number of nearest neighbours and  $T_1$  the hopping integral between neighbouring lattice sites. For the calculations in two dimensions we choose the dispersion of the square lattice:

$$\varepsilon(\mathbf{k}) = \frac{Z_1 T_1}{2} \left( \cos(k_x a) + \cos(k_y a) \right) + T_0. \quad (67)$$

Throughout this section, we fix the Bloch-bandwidth to  $W = -2Z_1 T_1 = 2 \text{ eV}$  and the center of gravity of the Bloch band to  $T_0 = 0 \text{ eV}$ . The corresponding BDOS are plotted in Fig. 1.

Out of the infinite number of possible antiferromagnetic structures, we consider only the relatively simple and most commonly used ones, AFM-(110) and AFM-(AB), which are shown in Fig. 2. Within the tight-binding approximation the hopping integrals  $T_{ij}^{\alpha\beta}$  read and the corresponding Bloch energies (18) are given by:

$$\epsilon_{AA}^{(110)}(\mathbf{k}) = \epsilon_{BB}^{(110)}(\mathbf{k}) = T_0 + 2T_1 \left[ \cos\left(\frac{a}{2}(k_x + k_y - k_z)\right) + \cos\left(\frac{a}{2}(-k_x + k_y + k_z)\right) \right], \quad (68)$$

$$\epsilon_{AB}^{(110)}(\mathbf{k}) = (\epsilon_{BA}^{(110)})^*(\mathbf{k}) = 2T_1 e^{i\mathbf{k} \cdot (\mathbf{r}_A - \mathbf{r}_B)} \times \left[ \cos\left(\frac{a}{2}(k_x + k_y + k_z)\right) + \cos\left(\frac{a}{2}(k_x - k_y + k_z)\right) \right], \quad (69)$$

and

$$\epsilon_{AA}^{(AB)}(\mathbf{k}) \equiv 0, \quad (70)$$

$$\epsilon_{AB}^{(AB)}(\mathbf{k}) = T_1 e^{i\mathbf{k} \cdot (\mathbf{r}_A - \mathbf{r}_B)} \times \cos\left(\frac{k_x a}{2}\right) \cos\left(\frac{k_y a}{2}\right) \cos\left(\frac{k_z a}{2}\right). \quad (71)$$

### A. Paramagnetism

In Fig. 3 the QDOS in three and two dimensions are plotted for both cases, with and without the  $\mathbf{k}$ -dependent term  $F_{\mathbf{k}-\sigma}$  of the self-energy. The quasiparticle spectrum is divided into two parts, a low and a high energy region. These two quasiparticle subbands (so-called Hubbard-bands) are separated by an energy amount comparable to the intraatomic Coulomb matrix element  $U$ . The inclusion of the  $\mathbf{k}$ -dependent term  $F_{\mathbf{k}-\sigma}$  into the self-energy leads to a band narrowing which gets stronger with increasing band occupation. Since the centers of gravity of the subbands remain almost constant the energy gap between the subbands increases. As can be seen in Fig. 3, the band narrowing effect gets much stronger as the dimension is lowered from three to two. Since, in principle, magnetism is favoured by narrow energy bands one expects the magnetic region to be enhanced by taking the non-locality of the self-energy into account. The band narrowing effect holds for the attractive Hubbard model ( $U < 0$ ) as well. Contrary to the suggestions in<sup>33</sup>, the two Hubbard bands do not melt together as the non-local part of the self-energy is included.

Further insight into the effect of the non-local term of the self-energy can be obtained from the quasiparticle dispersion which is shown in Fig. 4 for the two-dimensional system and moderate Coulomb interaction  $U = W$ . The band narrowing of the lower Hubbard-band is mainly due to a flattening of the dispersion near (1,1). The flattening extends to the saddle point (1,0) and halfway to (0,0). For half filling the inclusion of the  $\mathbf{k}$ -dependence even leads to a local minimum of the dispersion at (1,1).

Recently, this flattening of the bands has been discussed in connection with high temperature superconductivity<sup>47,23</sup>, because similarly flat dispersions are seen in angle resolved photoemission experiments on hole-doped cuprate superconductors. Beenen and Edwards<sup>23</sup> show that quasiparticle dispersions like the ones in Fig. 4 compare rather well with quantum monte carlo simulations for a  $4 \times 4$ -cluster<sup>43,44</sup>. Similar results for one dimension are given in<sup>37</sup> where the authors argue that the inclusion of the non-local terms is crucial for a good agreement of the model calculation with exact diagonalization results for a 10-site Hubbard-ring.

For the complete information about the quasiparticle spectrum one has to look at both, the quasiparticle energies  $E_{j\sigma}(\mathbf{k})$  and the corresponding spectral weights  $\alpha_{j\sigma}(\mathbf{k})$ . The spectral weight  $\alpha_{1\sigma}(\mathbf{k})$  of the lower quasiparticle subband is shown in the lower part of Fig. 4. The spectral weight of the upper subband is given by

$\alpha_{2\sigma}(\mathbf{k}) = 1 - \alpha_{1\sigma}(\mathbf{k})$ . If one introduces holes into the half filled system, there is a strong transfer of spectral weight from the upper to the lower subband. This weight transfer is particularly prominent around (1,1).

Now, we want to focus on the bandwidth correction and the three correlation functions contained therein. In Fig. 5 these correlation functions are plotted for the three-dimensional case as a function of  $n$  for three different values of  $U$ . All correlation functions are negative and disappear, of course, in the empty band limit ( $n = 0$ ) because of the lack of interaction partners.

The double hopping correlation function is rather small and vanishes completely for  $U \rightarrow \infty$  due to the unfavourable double occupancies. Since double hopping processes require a double occupied and an empty site, the double hopping correlation function exhibits a weak maximum at quarter filling and disappears at half filling and not too small values of  $U$  (here and in the following we refer to the absolute values of the correlation functions). The double hopping correlation plays, therefore, a minor role in the following.

Of greater importance with respect to the  $\mathbf{k}$ -dependence are the density and the spinflip correlation. Both correlation functions increase in a wide region of the band occupation  $n$  monotonously with increasing  $n$  and are, in this region, nearly independent of  $U$ . Close to half filling and for  $U > W$ , however, this behaviour changes and both correlation functions are strongly reduced. This is because near half filling and not too small values of  $U$  the hopping between nearest neighbours is suppressed. If the lower Hubbard-band gets filled, hopping is possible only via double occupancies.

In the case of exact half filling ( $n = 1$ ), however, the density and spinflip correlation, and therefore  $F_{-\sigma}$ , have a finite value for all  $U$ . The behaviour of  $n_{-\sigma}(1 - n_{-\sigma})F_{-\sigma}$  is shown in the inset in Fig. 5. For  $U = 5.0 \text{ eV}$  a smooth transition to the value at half filling is indicated, although we do not find fully converged numerical solutions as  $n \lesssim 1$ . For  $U \rightarrow \infty$  this transition becomes discontinuous, indicating that the two limits  $n \rightarrow 1$  and  $U \rightarrow \infty$  do not commute (see Sec. IV). For not too small  $U$  and half filling, the numerical calculations reproduce  $F_{-\sigma} = -3/Z_1$  given by (64) quite accurately.

From Fig. 5 one obtains that almost all the effect of the density and spinflip correlation is gathered in the spin-spin correlation function  $\langle \mathbf{S}_i \mathbf{S}_j \rangle$  which indicates antiferromagnetic correlations between nearest neighbours.

In Fig. 6 the bandwidth correction is shown in one, two and three dimensions. The bandwidth correction clearly gets less important as the dimension increases. This fits perfectly well into the picture developed by the investigations of the Hubbard model for infinite dimensions where the self-energy becomes local<sup>11</sup>. The SDA reproduces the locality of the self-energy in the limit  $d \rightarrow \infty$ .

### B. Spontaneous magnetism

**Magnetic phase diagram:** The global results of our calculations are summarized in the magnetic phase dia-



gram, which is shown in Fig. 7. We restrict the phase diagram to the region  $0 \leq n \leq 1$ , since due to particle-hole symmetry the phase diagram is symmetric to the  $n = 1$  axis.

Within the SDA, we find in wide parameter regions ferromagnetic and antiferromagnetic solutions besides the ever existing paramagnetic one. If there is more than one mathematical solution of the system, the physically stable one is indicated by the minimum free energy. Spontaneous magnetism is possible only for  $n$  greater than a critical band occupation  $n_c(U)$ . As  $U$  increases  $n_c$  decreases slightly without getting smaller than  $n_0 = 0.54$ . This is consistent with the results obtained by Kanamori<sup>48</sup>. Here, we see the qualitative improvement of the SDA upon a simple, but often used Hartree-Fock approximation (Stoner model)<sup>49</sup>, where magnetic solutions can be found for all band occupations as long as the Coulomb interaction  $U$  is strong enough<sup>22,50</sup>. The Hartree-Fock approximation is well known to overestimate the possibility of spontaneous magnetism.

Besides a critical value for the band occupation, also a critical Coulomb interaction  $U_c$  is needed to build up spontaneous ferromagnetic solutions.  $U_c^{\text{FM}}$  has a minimum at  $n = 0.75$ , where, consistent with the Stoner criterion, the chemical potential  $\mu$  lies in the region of maximum density of states.  $U_c^{\text{AFM-(110)}}$  is slightly bigger than the Bloch-bandwidth  $W$ . However, antiferromagnetism in the AFM-(110) configuration is energetically stable only in a small region below the ferromagnetic phase. Antiferromagnetism in the AFM-(AB) configuration is observed for band occupations close to half-filling. We find stable AFM-(AB) solutions down to very small values of  $U$ . However, the question, if AFM-(AB) solutions exist even for  $U \rightarrow 0^+$  (as for the sc lattice, see for example<sup>20</sup>) can not reasonably be addressed within our strong coupling approach. In the limit of large  $U$ , the region, where antiferromagnetism in the AFM-(AB) configuration is stable against ferromagnetism, is reduced to a small corridor around  $n = 1$ . Altogether, antiferromagnetism is favoured by moderate Coulomb interaction  $U \approx W$ .

The stability of the AFM-(AB) phase for the half filled band  $n = 1$  can be explained as follows: Via second order perturbation theory the Hubbard model at half filling can be transformed into an effective Heisenberg model with exchange integrals equal to  $J_{ij} = -2(T_{ij})^2/U$  ( $i \neq j$ )<sup>51</sup>. Therefore, the total energy of the system is lowered by virtual hopping processes where an electron hops from lattice site  $i$  to a neighbouring site  $j$  and back to  $i$  again<sup>50</sup>. For this virtual processes to be possible, the quasiparticles on neighbouring sites need to have reversed spins because of the Pauli exclusion principle. Thus the lowering of the total energy is determined by the number of neighbouring sites occupied with reversed spin quasiparticles. This number is highest in the AFM-(AB) configuration, followed by AFM-(110), PM and being zero for FM. This corresponds exactly to the results of our numerical calculations.

Applying a modified perturbation theory (SOPT-HF: second order perturbation theory around the Hartree-

Fock solution) Bulk and Jelitto<sup>52</sup> derive a qualitatively very similar phase diagram. In particular, their calculations yield similar values for the critical parameter  $n_c$  and  $U_c^{\text{FM}}$ . This is a remarkable result, because perturbation theory is usually restricted to very small values of  $U$ , whereas the SDA does best in the strong coupling region. The qualitative agreement between SDA and modified perturbation theory, therefore, leads to the conclusion that both theories produce reliable results with respect to magnetism for moderate Coulomb interaction  $U \simeq W$  as well.

**Ferromagnetism:** In Fig. 8 the magnetization  $m$  of the ferromagnetic system is plotted as a function of  $n$  for various values of  $U$ . In addition the inverse static, paramagnetic susceptibility  $(\chi^{(0)}(n, T))^{-1}$  is shown.  $(\chi^{(0)}(n, T))^{-1}$  has either none or two roots which correspond to the instabilities of the system against ferromagnetic order. The roots of  $(\chi^{(0)}(n, T))^{-1}$ , which has been calculated from the paramagnetic solution only, indicate exactly the second order phase transitions between paramagnetism and ferromagnetism. As  $U$  increases the magnetic solutions start from lower band occupations and show a higher magnetization. However, there are two different behaviours: For  $U < 2.8$  eV the magnetization curves have a maximum around  $n \simeq 0.8$  and exist only between the two roots of  $(\chi^{(0)}(n, T))^{-1}$ . But this behaviour only occurs in a parameter region, where ferromagnetism is unstable against paramagnetism. Above  $U \geq 2.8$  eV we find two ferromagnetic solutions FM1 and FM2, which start at the roots of  $(\chi^{(0)}(n, T))^{-1}$  and exist both until  $n = 1$ . By looking at the free energy we can conclude that FM1 is always energetically favourable against FM2<sup>41</sup>. As  $n$  increases, the FM1 solutions reach the ferromagnetic saturation  $m = n$ . In the limit  $U \rightarrow \infty$  the system is fully polarized above  $n = 0.65$ .

In Fig. 8 we also show a magnetization curve for  $U = 5$  eV without the  $\mathbf{k}$ -dependent term  $F_{\mathbf{k}-\sigma}$  of the self-energy. As expected, magnetism is favoured by inclusion of the  $\mathbf{k}$ -dependence. Nevertheless, in three dimensions the influence of the  $\mathbf{k}$ -dependence on the magnetic properties is rather small. The qualitative behaviour of the system with and without  $F_{\mathbf{k}-\sigma}$  is very similar. The same is valid in the case of antiferromagnetism.

We now want to focus on the temperature dependence of the magnetization which is plotted in Fig. 9 as a function of  $n$  for different temperatures  $T$  and in Fig. 10 as a function of  $T$  and various band occupations  $n$ . As  $T$  increases the magnetization clearly decreases. Near half filling the two ferromagnetic solutions FM1 and FM2 melt together. This causes first order phase transitions of the magnetization as a function of  $T$  for band occupations close to  $n = 1$  (see for example the  $n = 0.9$  curve in Fig. 10). Note that, again, the energetically stable solution is always the one with the higher magnetic moment. In Fig. 10 one can see that there are magnetic solutions that exist for higher temperatures than all Curie-temperatures corresponding to second order phase transitions. This explains the island-like behaviour of the  $T = 600$  K curve in Fig. 9. For  $n \leq 0.7$  all magnetization

curves  $m(T)$  show a second order phase transition with a shape very similar to a Brillouin function, as in localized moment Heisenberg ferromagnets.

From the magnetization curves  $m(T)$  as well as from  $(\chi^{(0)}(n, T))^{-1}$  we can determine the Curie temperatures  $T_C$  which are shown in Fig. 11. As a function of  $n$  the Curie-temperatures are highest in the region around  $n \simeq 0.75$ . Because the two ferromagnetic solutions FM1 and FM2 melt together for very low temperatures as  $n$  approaches half filling, the Curie-temperatures reduce to zero at  $n = 1$ . In Fig. 11(a) we also show the roots of the inverse static susceptibility. The system exhibits first order phase transitions as soon as both curves are disjunct.

For a given band filling  $n$ , the Curie temperature increases with the Coulomb interaction  $U$ , but saturates in the limit  $U \rightarrow \infty$  at a finite value which depends on  $n$ . We want to emphasize that this behaviour is a decisive improvement upon the Stoner model of band magnetism, for which  $T_C$  is unrealistically high and increases linearly with  $U$ <sup>22</sup>.

For a better understanding of the macroscopic magnetic properties like  $m$  and  $T_C$ , it is useful to look at the quasiparticle density of states and quasiparticle dispersion. These are plotted in Fig. 12 for  $T = 0$  K and  $U = 5.0$  eV. In Fig. 12(a) the QDOS is shown for four different band occupations. For  $n = 0.55$  there is no ferromagnetic solution and the QDOS consists of two quasiparticle peaks corresponding to the lower and upper Hubbard-bands. If the band occupation exceeds  $n = 0.58$ , however, an additional spin-splitting occurs between  $\rho_\uparrow$  and  $\rho_\downarrow$  which leads to ferromagnetism. There are essentially two distinct correlation effects in the QDOS: An energy shift between the centers of gravity of the  $\uparrow$  and the  $\downarrow$  subbands (Stoner shift) and a deformation of the density of states. The band deformation is directly connected to a transfer of spectral weight between the upper and lower quasiparticle subbands. The energy shift and the deformation of the band are strongly  $n$  and  $T$  dependent. Both effects together determine the spin-asymmetry of the QDOS and, therefore, the magnetic properties of the system. In particular, near the upper edge of the lower quasiparticle subband, the interplay between the band shift and the band deformation leads to an inverse exchange splitting, i.e the  $\downarrow$  quasiparticle states are energetically below the  $\uparrow$  states. This is because the band narrowing of the lower minority band overcompensates the Stoner shift.

Qualitatively, the band deformation and the transfer of spectral weight is easy to understand: The lower quasiparticle band results from electron hopping over lattice sites which are not occupied by electrons with opposite spin. For non-zero magnetization, the number of these sites becomes spin dependent. The probability of finding a majority electron on an otherwise empty site is enhanced for  $m > 0$ . Thus the lower  $\rho_\downarrow$ -band is narrowed as  $m$  increases and finally vanishes in the ferromagnetic saturation and  $n \rightarrow 1$ . The lower majority subband, however, is broadened with decreasing number of minority particles until it becomes, for  $m = n$ , equal to the BDOS because of missing interaction partners. As can be seen

analytically in the strong coupling limit, the weight of the lower ( $\sigma$ )-spin quasiparticle subband roughly scales with  $(1 - n_{-\sigma})$ . The weight of the upper subband, where the hopping of the electrons is essentially via lattice sites which are already occupied by a reversed spin electron, scales with  $n_{-\sigma}$ .

The temperature dependence of the QDOS and the corresponding quasiparticle dispersions are shown in Fig. 12(b),(c). The spin asymmetry of the partially filled lower quasiparticle subband decreases with increasing temperature. This is, again, partly due to a Stoner-shift and partly due to a deformation of the subbands. For temperatures above  $T_C$ , the spin-splitting, of course, vanishes, but the upper and lower parts of the spectrum remain separated by a gap of order  $U$ .

The spin-splitting of the quasiparticle dispersion (Fig. 12(c)) scales with the magnetization. However, the actual amount of the spin-splitting strongly depends on the position in the Brillouin zone. There even is a region in  $\mathbf{k}$ -space, where the quasiparticle energies are nearly independent of  $T$ . Near the upper edge of the lower quasiparticle subband the above mentioned inverse exchange splitting is clearly visible.

In the inset in Fig. 12(c) the spectral weight of the lower peak in the spectral density is shown. For  $T = 0$  K the spectral weight is strongly spin dependent. As the temperature increases, a redistribution of spectral weight between the upper and lower subband leads to a decrease of this asymmetry. From Fig. 12(c) follows that a conventional  $E_\sigma(\mathbf{k})$  band-structure representation does not contain the full information about the underlying system, because details about the distribution of spectral weight are missing.

The spin asymmetry of the QDOS is due to the correction term  $B_{\mathbf{k}-\sigma}$  in the self-energy which is given by the bandshift  $B_{-\sigma}$  and the bandwidth correction  $F_{-\sigma}$ . With respect to the strong correlation limit, we have plotted in Fig. 13 the effective bandshift  $n_{-\sigma}B_{-\sigma}$  and the effective bandwidth correction  $n_{-\sigma}F_{-\sigma}$  as a function of  $n$ . Note that  $n_\downarrow B_\downarrow$  is the effective bandshift of the lower  $\uparrow$ -subband. The same holds for  $n_{-\sigma}F_{-\sigma}$ .

For  $n$  larger than  $n = 0.58$  the effective bandshift becomes strongly spin dependent, allowing, therefore, for the existence of ferromagnetism. The effective bandshift of the majority band becomes very small and disappears in the ferromagnetic saturation due to  $n_\downarrow = 0$ . The effective bandshift of the minority band, however, increases rapidly and tends towards  $W/2 = 1.0$  eV as  $n \rightarrow 1$ . The minority band gets, therefore, shifted above the Fermi edge.

The spin asymmetry of the effective bandwidth correction is less pronounced. This is because only the density correlation is spin dependent. Further,  $n_{-\sigma}F_{-\sigma}$  vanishes in the case of half filling. This is consistent with the analytical results of section IV.

**Antiferromagnetism:** The sublattice magnetizations  $m_A$  for different temperatures  $T$  are plotted in Fig. 14 (a) and (b) for the AFM-(110) and the AFM-(AB) configurations respectively. The most striking difference

to the ferromagnetic system is that the sublattice magnetizations never reach the saturation  $m_A = n$ . This is because in an antiferromagnetic system the spin up and spin down density of states occupy exactly the same energy region. Filling the subbands with particles up to the Fermi level, therefore, always leads to a non-vanishing number of particles with minority spin, resulting in  $m_A < n$ .

The temperature dependence of  $m_A$  in the AFM-(110) phase is quite similar to the one in the case of ferromagnetism. This does not hold for the AFM-(AB) configuration, which is particularly stable near half filling. The two solutions AFM1 and AFM2 in the AFM-(AB) phase stay separated and do not melt together until fairly high temperatures. This can be understood by means of the sublattice density of states which are discussed later. The chemical potentials  $\mu_1, \mu_2$  of the AFM1 and AFM2 solutions are separated in the AFM-(AB) phase by the so-called Slater gap. For AFM1 and AFM2 to melt together, the broadening of the Fermi function has to be comparable to the size of the Slater gap.

In Fig. 15 the Néel temperatures are shown as a function of Coulomb interaction  $U$ . In the AFM-(AB) configuration the Néel temperatures are highest for moderate Coulomb interaction, they decrease with increasing  $U$  in the strong coupling region and converge to a finite value as  $U \rightarrow \infty$ . The maximum is most pronounced for band occupations close to half filling. As already mentioned, for the half filled band the Hubbard model can be transformed via second order perturbation theory into an effective Heisenberg model with antiferromagnetic exchange integrals  $J_{ij} = -2(T_{ij})^2/U^{51,53}$ . Thus, using the mean field approximation for the Heisenberg model, one finds  $T_N \sim 1/U$ . Close to half-filling and for not too small values of  $U$  the  $T_N(U)$  curves in the AFM-(AB) phase show, at least qualitatively, this behaviour. In the AFM-(110) configuration, which is built by alternating ferromagnetic planes, the decrease of the Néel temperatures as the Coulomb interaction increases is only weak. Here again, antiferromagnetism in the AFM-(110) configuration behaves quite similar to ferromagnetism.

The sublattice density of states of the two antiferromagnetic configurations is shown in Fig. 16. Contrary to the ferromagnetic system,  $\rho_{A\uparrow}(E)$  and  $\rho_{A\downarrow}(E)$  occupy exactly the same energy region due to the spin independence of the quasiparticle energies. The spectral weights which are connected to the quasiparticle energies show, however, a spin asymmetry leading to a spin dependent density of states. As for the paramagnetic and the ferromagnetic system there is the splitting of the density of states into the lower and the higher energy region separated by  $U$ . In the AFM-(AB) phase an additional Slater gap occurs in the sublattice density of states for all parameters, due to the high symmetry of the magnetic Brillouin zone. This Slater gap is not visible in the AFM-(110) configuration. As the sublattice magnetization  $m_A$  increases, the shape of the sublattice density of states in the AFM-(110) phase becomes more and more similar to the density of states of a two-dimensional system with sharp edges and a logarithmic singularity at the center. This quasi two-dimensionality originates from the ferro-

magnetic ordered planes in the AFM-(110) configuration (see Fig. 2).

## VI. SUMMARY AND CONCLUSIONS

We presented a self-consistent moment approach to the Hubbard model which is based on a two pole ansatz for the one electron spectral density. A complete evaluation of this theory, which does not involve any further approximations, leads to results identical to the method proposed by Roth. We believe, however, the SDA to be physically more transparent and better motivated, due to the analysis in the strong coupling limit, which were essential to formulate the two-pole ansatz. Since the SDA reproduces the band limit, the atomic limit and the strong coupling limit, it is expected to provide a reasonable interpolating solution covering the intermediate and strong coupling regime. This is confirmed in the paramagnetic case by the excellent agreement between the quasiparticle energies calculated with the SDA and recent Quantum Monte Carlo results<sup>43,44</sup>. For the ferromagnetic case we find a phase diagram very similar to the modified perturbation theory (SOPT-HF)<sup>52</sup>, which does best for weak and intermediate Coulomb interaction.

From the presented phase diagram we read off, that spontaneous ferromagnetism exists only above a critical value of the band occupation and the Coulomb interaction. Therefore, the SDA is much more restrictive than a simple mean field theory (Stoner model). Antiferromagnetism is most stable for intermediate coupling strength  $U \approx W$  and in a small region around  $n = 1$ . As a function of temperature the magnetization curves show second order phase transitions away from half filling. For band occupations close to half filling, however, the system exhibits first order transitions to the paramagnetic phase. Note, that these first order transitions can not be observed by looking at the poles of the static paramagnetic susceptibility. The corresponding critical temperatures  $T_C$  and  $T_N$  lie for all parameters in a physically reasonable region. All magnetic properties of the Hubbard model were shown to find a direct explanation in the  $(n, T, U)$ -dependent QDOS.

By investigation of the system with and without the non-local term in the self-energy, we find, that the inclusion of the  $\mathbf{k}$ -dependence leads to a narrowing of the quasiparticle subbands. The correlation functions, which represent the non-locality of the self-energy were discussed in detail. Here we found, that almost all effect of the  $\mathbf{k}$ -dependence is gathered in the spin-spin correlation, which turns out to be negative, indicating, therefore, antiferromagnetic correlation. Consistent with the  $d = \infty$  theory, the non-local terms rapidly become less important as the dimension  $d$  and the number of nearest neighbours  $Z_1$  increases. For the three-dimensional bcc lattice, the influence of the  $\mathbf{k}$ -dependent terms in the self-energy on the magnetic properties is only marginal, whereas in two dimensions the corrections due to the non-locality are essential. In two dimensions, however, we did restrict

our investigations to the paramagnetic case, since spontaneous magnetic order in the two-dimensional Hubbard model is excluded by the Mermin-Wagner theorem<sup>54,5</sup>. Very recent calculations indicate, that for the three-dimensional sc lattice the influence of the non-local terms with respect to ferromagnetism is much more important than for the bcc lattice. We will discuss this fact in a forthcoming paper, where we investigate the influence of the lattice structure on ferromagnetism in the Hubbard model<sup>32</sup>.

### ACKNOWLEDGMENTS

This work has been done within the Sonderforschungsbereich 290 ("Metallische dünne Filme: Struktur, Magnetismus und elektronische Eigenschaften") of the Deutsche Forschungsgemeinschaft.

- 
- <sup>1</sup> J. Hubbard, Proc. R. Soc. London, Ser. A **276**, 238 (1963).
  - <sup>2</sup> N. F. Mott, Proc. R. Soc. London, Ser. A **62**, 416 (1949).
  - <sup>3</sup> J. Hubbard, Proc. R. Soc. London, Ser. A **281**, 401 (1964).
  - <sup>4</sup> E. Lieb and F. Wu, Phys. Rev. Lett. **20**, 1445 (1968).
  - <sup>5</sup> D. K. Ghosh, Phys. Rev. Lett. **27**, 1584 (1971).
  - <sup>6</sup> Y. Nagaoka, Phys. Rev. **147**, 392 (1966).
  - <sup>7</sup> E. H. Lieb, Phys. Rev. Lett. **62**, 1201 (1989).
  - <sup>8</sup> L. M. Roth, Phys. Rev. **184**, 451 (1969).
  - <sup>9</sup> W. Nolting, Z. Phys. B - Condens. Matter **255**, 25 (1972).
  - <sup>10</sup> P. W. Anderson and J. R. Schrieffer, Physics Today **44**, 55 (1991).
  - <sup>11</sup> W. Metzner and D. Vollhardt, Phys. Rev. Lett. **62**, 324 (1989).
  - <sup>12</sup> E. Müller-Hartmann, Z. Phys. B - Condens. Matter **74**, 507 (1989).
  - <sup>13</sup> D. Vollhardt, *Proc. Int. School of Physics "Enrico Fermi", Course CXXI*, eds R. A. Broglia and J. R. Schrieffer, North-Holland, Amsterdam, p.31 (1994).
  - <sup>14</sup> V. Janis and D. Vollhardt, Int. J. Mod. Phys. B **6**, 731 (1992).
  - <sup>15</sup> M. Jarrell, Phys. Rev. Lett. **69**, 168 (1992).
  - <sup>16</sup> A. Georges and G. Kotliar, Phys. Rev. B **45**, 6479 (1992).
  - <sup>17</sup> E. Müller-Hartmann, Th. Hanisch, and R. Hirsch, Physica B **186-188**, 834 (1993).
  - <sup>18</sup> G. S. Uhrig, Phys. Rev. Lett. **77**, 3629 (1996).
  - <sup>19</sup> M. Ulmke, preprint cond-mat 9512044
  - <sup>20</sup> R. T. Scalettar, D. J. Scalapino, R. L. Sugar, and D. Trounsaint, Phys. Rev. B **39**, 4711 (1995).
  - <sup>21</sup> J. K. Freericks and M. Jarrell, Phys. Rev. Lett. **74**, 186 (1995).
  - <sup>22</sup> W. Nolting and W. Borgiel, Phys. Rev. B **39**, 6962 (1989).
  - <sup>23</sup> J. Beenen and D. M. Edwards, Phys. Rev. B **52**, 13636 (1995).
  - <sup>24</sup> H. Mori, Prog. Theor. Phys. **33**, 423 (1965).
  - <sup>25</sup> R. Zwanzig, Phys. Rev. **124**, 983 (1961).
  - <sup>26</sup> W. Nolting and A. M. Oleś, Physica **143A**, 296 (1973).
  - <sup>27</sup> L. S. Campana, A. Caramico D'Auria, M. D'Ambrosio, L. De Cesare, and U. Esposito, Physica **123A**, 279 (1984).
  - <sup>28</sup> L. A. B. Bernardes, O. N. Borges, and L. A. A. Riberio, phys. stat. sol. (b) **135**, 581 (1986).
  - <sup>29</sup> M. Potthoff and W. Nolting, J. Phys.: Condens. Matter **8**, 4937 (1996).
  - <sup>30</sup> H. Eskes, A. M. Oleś, M. B. J. Meinders, and W. Stephan, Phys. Rev. B **50**, 17980 (1994).
  - <sup>31</sup> Besides ferromagnetic and commensurate antiferromagnetic order, also incommensurate antiferromagnetic order is possible in the Hubbard model (see for example<sup>21</sup>). Such calculations are not included here and are left for future study.
  - <sup>32</sup> T. Herrmann and W. Nolting, Solid State Commun. **to be published** (1997).
  - <sup>33</sup> T. Schneider, M. H. Pedersen, and J. J. Rodríguez-Núñez, Z. Phys. B - Condens. Matter **100**, 263 (1996).
  - <sup>34</sup> M. Maška, Phys. Rev. B **48**, 1160 (1993).
  - <sup>35</sup> M. Potthoff and W. Nolting, Phys. Rev. B **in press** (1997).
  - <sup>36</sup> M. Potthoff and W. Nolting, Surf. Sci. **in press** (1997).
  - <sup>37</sup> B. Mehlig, H. Eskes, R. Hayn, and M. B. J. Meinders, Phys. Rev. B **52**, 2463 (1995).
  - <sup>38</sup> A. B. Harris and R. V. Lange, Phys. Rev. **157**, 295 (1967).
  - <sup>39</sup> The influence of the Kondo peak on the magnetic behaviour of the Hubbard model will be discussed in a forthcoming paper: M. Potthoff, T. Wegener, and W. Nolting **to be published**, (1997).
  - <sup>40</sup> M. Jarrell and Th. Pruschke, Z. Phys. B - Condens. Matter **90**, 187 (1993).
  - <sup>41</sup> G. Geipel and W. Nolting, Phys. Rev. B **38**, 2608 (1988).
  - <sup>42</sup> S. Bei der Kellen, W. Nolting, and G. Borstel, Phys. Rev. B **42**, 447 (1990).
  - <sup>43</sup> N. Buluth, D. J. Scalapino, and S. R. White, Phys. Rev. B **50**, 7215 (1994).
  - <sup>44</sup> N. Buluth, D. J. Scalapino, and S. R. White, Phys. Rev. Lett. **73**, 748 (1994).
  - <sup>45</sup> T. Herrmann and W. Nolting, Phys. Rev. B **53**, 10579 (1996).
  - <sup>46</sup> W. Nolting, S. Bei der Kellen, and G. Borstel, Phys. Rev. B **43**, 1117 (1991).
  - <sup>47</sup> E. Dagotto, Rev. Mod. Phys. **66**, 763 (1994).
  - <sup>48</sup> J. Kanamori, Prog. Theor. Phys. (Kyoto) **30**, 275 (1963).
  - <sup>49</sup> E. C. Stoner, Proc. R. Soc. London, Ser. A **A154**, 656 (1936).
  - <sup>50</sup> M. Potthoff and W. Nolting, Phys. Rev. B **52**, 15341 (1995).
  - <sup>51</sup> P. W. Anderson, Solid State Phys. **14**, 99 (1963).
  - <sup>52</sup> G. Bulk and R. J. Jelitto, Phys. Rev. B **41**, 413 (1990).
  - <sup>53</sup> K. A. Chao, J. Spalek, and A. M. Oleś, J. Phys. C **10**, L271 (1977).
  - <sup>54</sup> N. D. Mermin and H. Wagner, Phys. Rev. Lett. **17**, 1133 (1966).

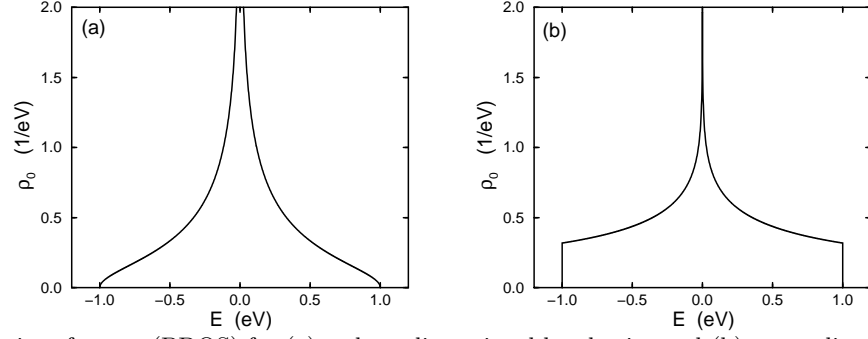


FIG. 1. Bloch density of states (BDOS) for (a) a three-dimensional bcc lattice and (b) a two-dimensional square lattice.

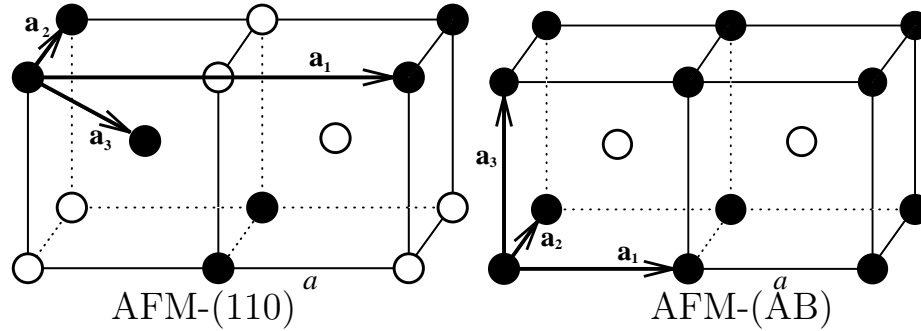


FIG. 2. Decomposition of the bcc lattice into two equivalent sublattices. The AFM-(110) configuration is built in such a way, that the (110)-planes alternately belong to the sublattice *A* and *B*. In the AFM-(AB) configuration all nearest neighbours of a given lattice site belong to the other sublattice. The vectors  $\mathbf{a}_{1,2,3}$  are the translation vectors of the respective magnetic Bravais lattice and *a* is the lattice constant.

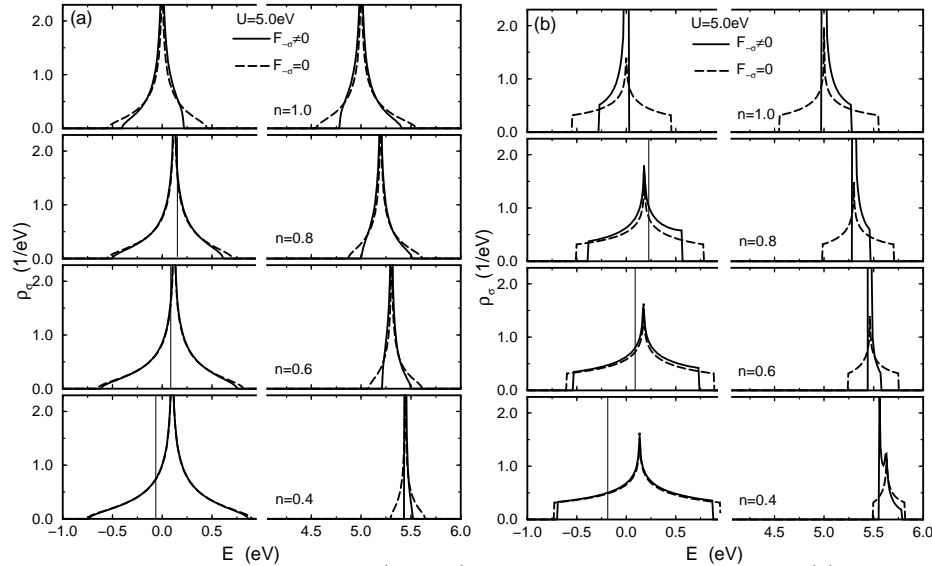


FIG. 3. Paramagnetic quasiparticle density of states (QDOS) as a function of the energy *E* in (a) three and (b) two dimensions for different band occupations *n* and the Coulomb interaction  $U = 5.0$  eV. Solutions with (solid lines) and without (broken lines) the non-local part of the electronic self-energy are shown. The vertical lines indicate the positions of the chemical potential  $\mu$ . ( $W = 2.0$  eV,  $T = 0$  K)

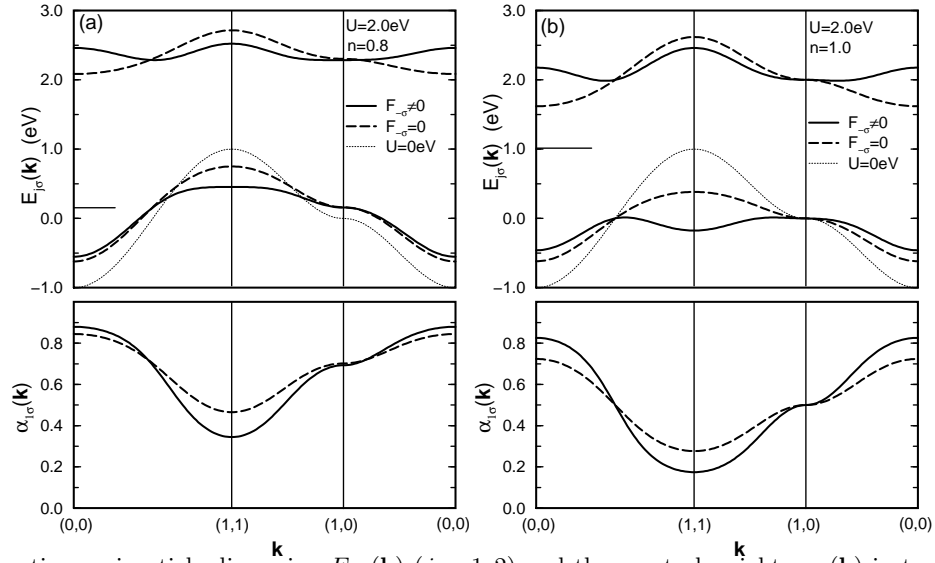


FIG. 4. Paramagnetic quasiparticle dispersion  $E_{j\sigma}(\mathbf{k})$  ( $j = 1, 2$ ) and the spectral weight  $\alpha_{1\sigma}(\mathbf{k})$  in two dimensions for the band occupations (a)  $n = 0.8$  and (b)  $n = 1.0$  and the Coulomb interaction  $U = 2.0$  eV. Solid lines: Solutions with included non-local part of the self-energy. Broken lines: Only the local part of the self-energy is taken into account. The dotted curve corresponds to the dispersion  $\varepsilon(\mathbf{k})$  of the Bloch band. The horizontal bars indicate the positions of the chemical potential  $\mu$ . The spectral weight of the upper quasiparticle subband is given by:  $\alpha_{2\sigma}(\mathbf{k}) = 1 - \alpha_{1\sigma}(\mathbf{k})$ . ( $W = 2.0$  eV,  $T = 0$  K)

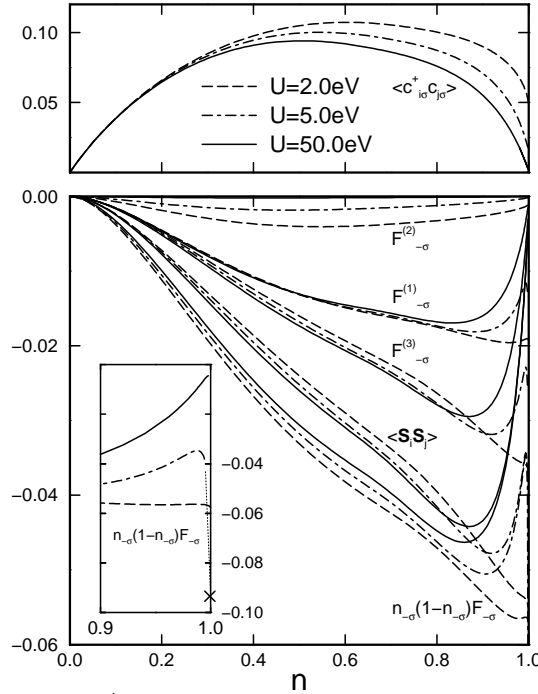


FIG. 5. Top: Hopping correlation function  $\langle c_{i\sigma}^\dagger c_{j\sigma} \rangle$  between nearest neighbours in three dimensions as a function of the band occupation  $n$  for various values of the Coulomb interaction  $U$ . Bottom: Density  $F_{-\sigma}^{(1)}$ , double hopping  $F_{-\sigma}^{(2)}$ , spinflip correlation  $F_{-\sigma}^{(3)}$  and the sum of these three correlation functions  $n_{-\sigma}(1-n_{-\sigma})F_{-\sigma}$  for the three-dimensional system as a function of  $n$  for various  $U$ . In addition, the spin-spin correlation function  $\langle \mathbf{S}_i \mathbf{S}_j \rangle$  is shown. In the inset, the limit  $n \rightarrow 1$  of  $n_{-\sigma}(1-n_{-\sigma})F_{-\sigma}$  is enlarged. ( $W = 2.0$  eV,  $T = 0$  K)

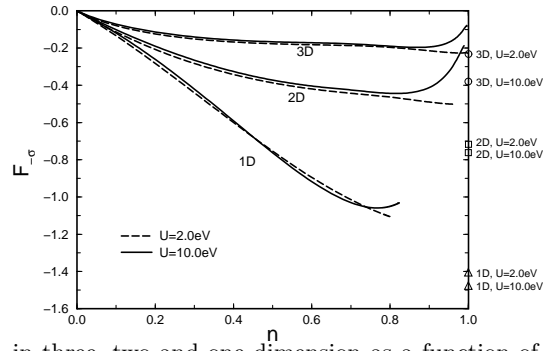


FIG. 6. Bandwidth correction  $F_{-\sigma}$  in three, two and one dimension as a function of the band occupation  $n$ . The values of  $F_{-\sigma}$  for half filling  $n = 1$  are given on the right. ( $W = 2.0$  eV,  $T = 0$  K)

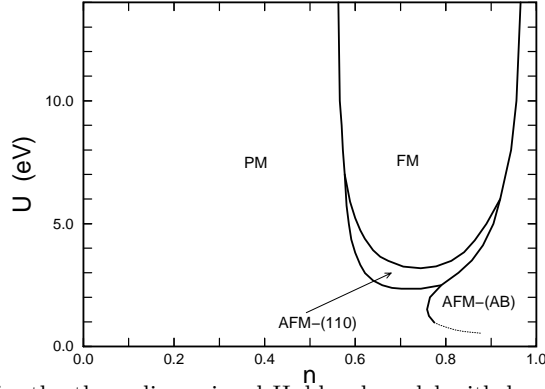


FIG. 7. Magnetic phase diagram for the three-dimensional Hubbard-model with bcc lattice structure.  $n$  is the band occupation and  $U$  the intraatomic Coulomb matrix element. The bandwidth of the BDOS is fixed to  $W = 2.0$  eV. Four phases are considered: Paramagnetism (PM), ferromagnetism (FM) and antiferromagnetism in two configurations AFM-(110) and AFM-(AB). ( $T = 0$  K)

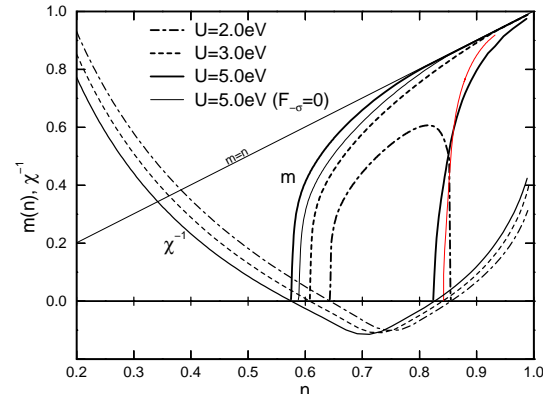


FIG. 8. Magnetization  $m$  as a function of the band occupation  $n$  for different Coulomb interactions  $U$ . In addition, the inverse static paramagnetic susceptibility  $(\chi^{(0)}(n, T))^{-1}$  is shown in arbitrary units. ( $W = 2.0$  eV,  $T = 0$  K)

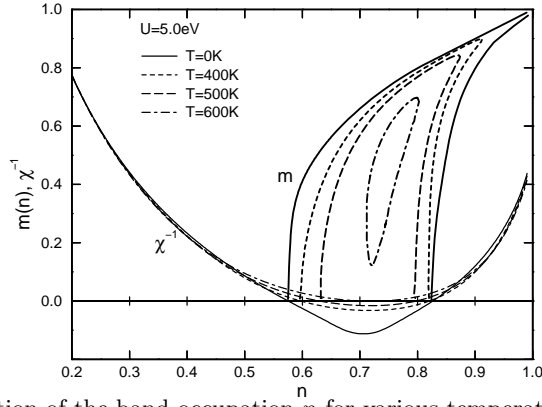


FIG. 9. Magnetization  $m$  as a function of the band occupation  $n$  for various temperatures  $T$ . In addition, the inverse static paramagnetic susceptibility  $(\chi^{(0)}(n, T))^{-1}$  is shown in arbitrary units. ( $U = 5.0$  eV,  $W = 2.0$  eV)

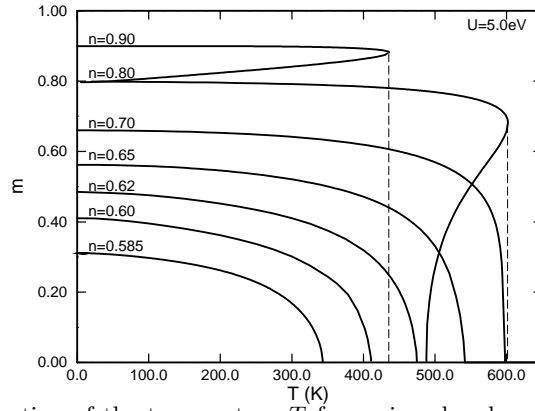


FIG. 10. Magnetization  $m$  as a function of the temperature  $T$  for various band occupations  $n$ . The dashed vertical lines indicate first order phase transitions. ( $U = 5.0$  eV,  $W = 2.0$  eV)

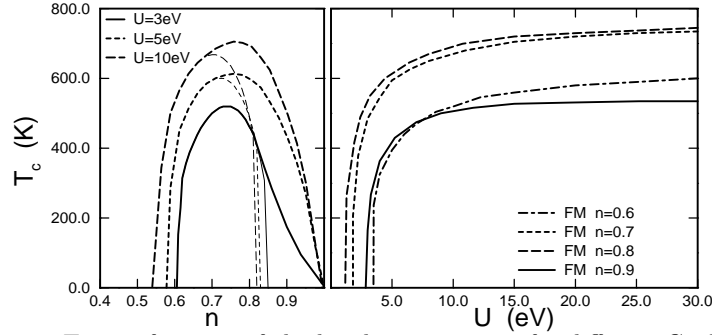


FIG. 11. (a) Curie-temperature  $T_c$  as a function of the band occupation  $n$  for different Coulomb interactions  $U$ . The thin dashed lines correspond to the roots of the inverse static susceptibility  $(\chi^{(0)}(n, T))^{-1}$ . (b) Curie-temperature  $T_c$  as a function of  $U$  for various  $n$ . ( $W = 2.0$  eV)



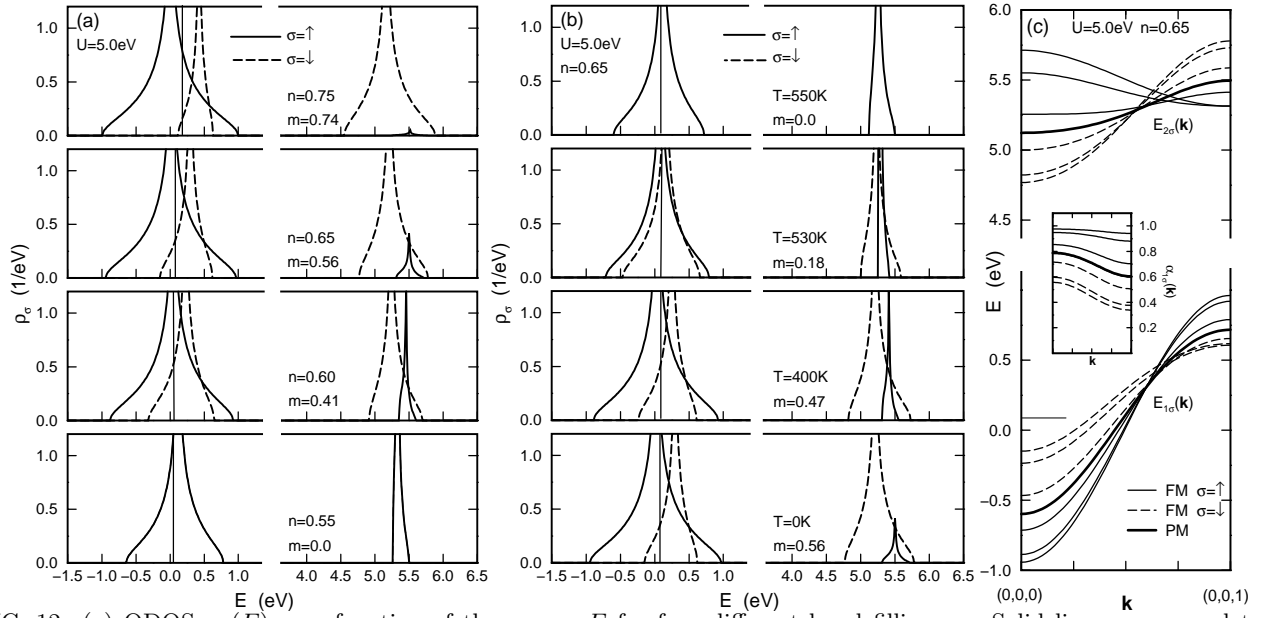


FIG. 12. (a) QDOS  $\rho_\sigma(E)$  as a function of the energy  $E$  for four different band fillings  $n$ . Solid lines correspond to the majority spin ( $\sigma=\uparrow$ ), broken lines to the minority spin direction ( $\sigma=\downarrow$ ). The vertical lines indicate the positions of the chemical potential  $\mu$ . (b) QDOS  $\rho_\sigma(E)$  for various temperatures  $T$ . (c) Quasiparticle dispersion  $E_{j\sigma}(\mathbf{k})$  for the same parameter as in (b) along the  $(0,0,1)$ -direction of the first Brillouin zone. In the inset, the spectral weight  $\alpha_{1\sigma}(\mathbf{k})$  is shown. From the outside to the inside:  $T = 0$  K,  $T = 400$  K,  $T = 530$  K and  $T = 550$  K; the thick line corresponds to the paramagnetic dispersion. ( $W = 2.0$  eV,  $T = 0$  K)

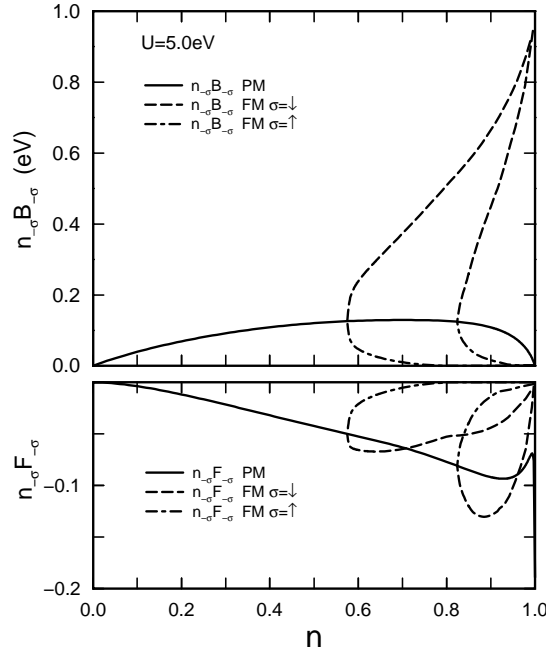


FIG. 13. Effective bandshift  $n_{-\sigma}B_{-\sigma}$  and effective bandwidth correction  $n_{-\sigma}F_{-\sigma}$  as a function of the band occupation  $n$  for the paramagnetic (PM) and the ferromagnetic (FM) phase. ( $W = 2.0$  eV,  $T = 0$  K)

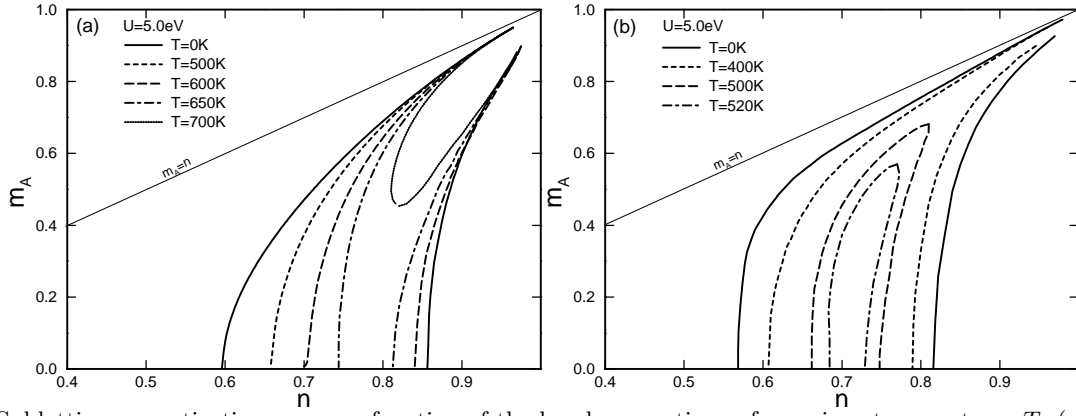


FIG. 14. Sublattice magnetization  $m_A$  as a function of the band occupation  $n$  for various temperatures  $T$ ; (a) AFM-(AB), (b) AFM-(110). ( $U = 5.0 \text{ eV}$ ,  $W = 2.0 \text{ eV}$ )

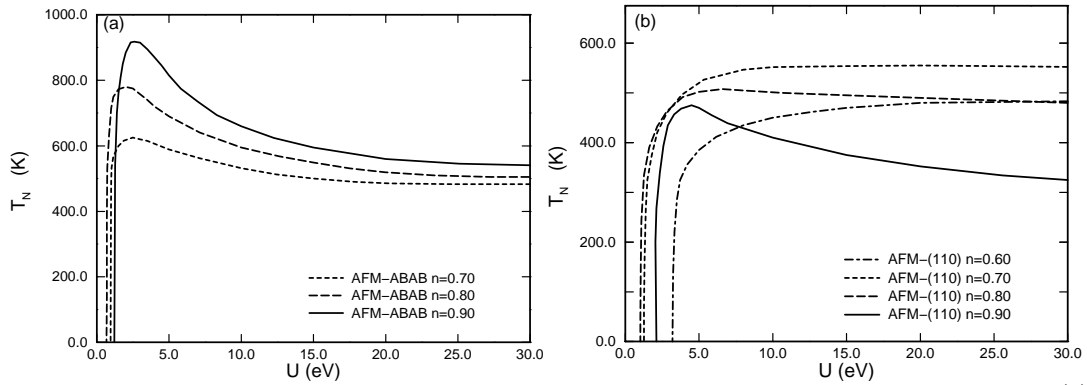


FIG. 15. Néel-temperatures  $T_N$  as a function of the Coulomb interaction  $U$  for different band occupations  $n$ ; (a) AFM-(AB), (b) AFM-(110). ( $U = 5.0 \text{ eV}$ ,  $W = 2.0 \text{ eV}$ )

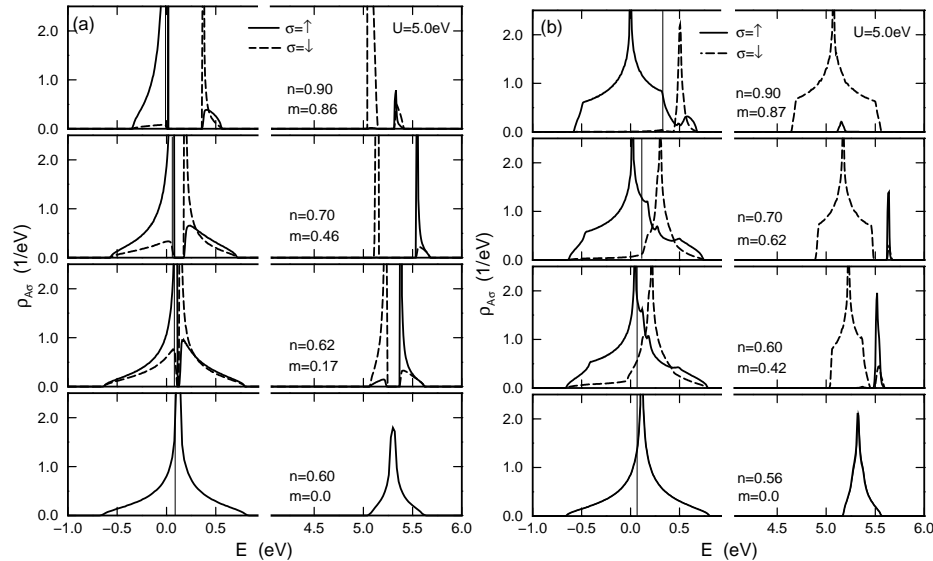


FIG. 16. Sublattice density of states  $\rho_{A\sigma}(E)$  for four different band occupations  $n$ ; (a) AFM-(AB), (b) AFM(110). Solid lines correspond to the majority spin ( $\sigma = \uparrow$ ), broken lines to the minority spin direction ( $\sigma = \downarrow$ ). The vertical lines indicate the positions of the chemical potential  $\mu$ . ( $W = 2.0 \text{ eV}$ ,  $T = 0 \text{ K}$ )